63107

P-43

NASA Technical Memorandum 110145

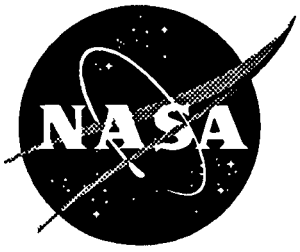

Analysis of Surface Cracks at Hole by a 3-D Weight Function Method with Stresses from Finite Element Method

W. Zhao
University of South Carolina, Columbia, South Carolina

J. C. Newman, Jr.
Langley Research Center, Hampton, Virginia

M. A. Sutton
University of South Carolina, Columbia, South Carolina

K. N. Shivakumar
North Carolina A&T State University, Greensboro, North Carolina

X. R. Wu
Institute of Aeronautical Materials, Beijing, Peoples Republic of China

July 1995

National Aeronautics and
Space Administration
Langley Research Center
Hampton, Virginia 23681-0001

Analysis of Surface Cracks at Hole by a 3-D Weight Function Method with Stresses from Finite Element Method

W. Zhao[1], J.C. Newman, Jr.[2], M.A. Sutton[1], K.N. Shivakumar[3] and X.R. Wu[4]

[1] *University of South Carolina, Columbia, SC 29208, U.S.A.*

[2] *NASA Langley Research Center, Hampton, VA 23681, U.S.A.*

[3] *North Carolina A & T State University, Greensboro, NC 27410, U.S.A.*

[4] *Institute of Aeronautical Materials, Beijing 100095, P.R. China*

ABSTRACT Parallel with the work in Part-I, stress intensity factors for semi-elliptical surface cracks emanating from a circular hole are determined. The 3-D weight function method with the 3-D finite element solutions for the uncracked stress distribution as in Part-I is used for the analysis. Two different loading conditions, i.e. remote tension and wedge loading, are considered for a wide range in geometrical parameters. Both single and double surface cracks are studied and compared with other solutions available in the literature. Typical crack opening displacements are also provided.

1. INTRODUCTION

Depending on the load and surface conditions of a hole, cracks may initiate and propagate approximately in the shapes of a quarter-elliptical corner crack, as discussed in [1], or a semi-elliptical surface crack, which will be addressed here. The first systematic solutions for surface cracked holes were available due to Grandt [2], who analyzed a single surface crack by a three-dimensional finite element alternating method. He considered two loading conditions, remote tension and crack face polynomial pressure up to the third degree. Using a three-dimensional finite element method, Newman and Raju [3] analyzed double surface cracks under remote tension for a wide range in geometry parameters. Based on their finite element results and engineering judgements, Newman and Raju [3] also developed a stress intensity factor equation, which has been widely used in various applications. More recently, Zhao et al [4] analyzed both

single and double surface cracks subjected to polynomial crack face pressure up to the fourth degree by the three-dimensional weight function method.

The present work is an extension to the previous one [4] by considering load variations in both plate width and plate thickness directions so as to incorporate the three-dimensional finite element solutions for the uncracked stress distribution into the weight function method, and by extending the weight function to cover relative crack depths up to a/t=0.9. By employing the uncracked stress distributions obtained from the three-dimensional finite element analysis for remote tension and wedge loading in the hole, stress intensity factors for these two loading conditions are determined. The geometrical parameters considered in this work are: r/t=0.2, 0.5, 1, 2, 3 and 5; a/c=0.2, 0.4, 1 and 2; a/t=0.01, 0.1, 0.2, 0.3, 0.4, 0.5, 0.6, 0.7, 0.8 and 0.9, within the limit of crack-length-to-hole-radius ratio of 2. Figure 1 shows the geometry being considered in this work. Both single crack and double cracks are considered, and the difference in stress intensity factors is evaluated. Comparisons of stress intensity factors determined by using 2-D and 3-D uncracked stress distributions are made. The results are compared with solutions available in the literature. Some typical crack face displacements are also provided and compared with those for 2-D cracks under appropriate limiting conditions.

NOMENCLATURE

a, c = semi-axes of a quarter-elliptical crack

a_x, c_y = crack length for a- and c-slices

b = half plate width

COD = dimensionless crack face displacement

E = elastic modulus

E_a, E_c = elastic modulus for a- and c-slices

E_s = elastic modulus for spring slices

F = dimensionless stress intensity factor

h = half plate height

k_a, k_c = stretching stiffness of restraining springs

K = stress intensity factor

K_a, K_c = stress intensity factors for a- and c-slices

P(x,y) = coupling force on the crack surface

Q = shape factor of an ellipse

r = hole radius

r_a, r_c = dimensionless restraining area for a- and c-slices

R_a, R_c = restraining area for a- and c-slices

t = half plate thickness

T = transition factor

V = crack face displacement

W_a, W_c = weight functions for a- and c-slices

x, y, z = Cartesian coordinates

η = an interpolation function at the free surface

ν = Poisson ratio

σ = remote tensile stress

σ_0 = a reference stress

φ = parametric angle of an elliptical crack

Φ = the complete elliptic integral of the second kind

2. THE 3-D WEIGHT FUNCTION METHOD

With the detailed description of the 3-D weight function method given in [1] for corner cracks, only a brief account in relation to surface cracks is given below for the double crack configuration.

Figure 1 shows the geometry of the problem to be considered (note the total plate thickness is 2t). In addition to remote tension, wedge loading in the hole will also be considered. Figure 2 shows the decomposition of the surface cracked body. Typical slices are depicted in

Fig. 3. The stiffness of the restraining springs, k_i (i=a,c), is a function of restraining area R_i, (i=a,c). The latter can be expressed in a non-dimensionalized form as

$$r_a=\frac{R_a}{c^2}=4\frac{a}{c}\left(\frac{b}{c}-\frac{r}{t}\frac{t}{a}\frac{a}{c}-1\right)\frac{t}{a} \tag{1a}$$

$$r_c=\frac{R_c}{a^2}=4\frac{c}{a}\left(\frac{b}{c}-\frac{r}{t}\frac{t}{a}\frac{a}{c}\right)\left(\frac{t}{a}-1\right) \tag{1b}$$

The k_i, (i=a,c), varies from 0 to ∞ as r_i varies from 0 to ∞. Figures 4 and 5 show the two limiting conditions as the stiffness of restraining springs tends to zero and infinity, respectively. These two limiting conditions serve as lower and upper bounds for the slices in Fig.3. Based on these bounding conditions, weight functions for the slices shown in Fig. 3 can be constructed as follows,

$$W_i=W_{2D,i}^{fixed}+T_i(r_i)\left(W_{2D,i}^{free}-W_{2D,i}^{fixed}\right) \tag{2}$$

where W_i (i=a,c) is the weight function for the slices in Fig. 3. $W_{2D,i}^{\ fixed}$ and $W_{2D,i}^{\ free}$ are the weight functions for the 2-D cracks with fixed boundary condition (Fig. 5) and with free boundary condition (Fig. 4), respectively. $T_i(r_i)$, designated as a transition factor, is an unknown function of restraining area, r_i, which satisfies $T_i(\infty)=0$, and $T_i(0)=1$.

We consider the case of infinite width, that is (c+r)/b=0. The particular weight functions W_i for our case are

$$W_a=W_{collinear}(a_x,y) \tag{3a}$$

$$W_c = W_{h2}(c_y, x) \tag{3b}$$

where $W_{collinear}$ is the weight function for collinear cracks and W_{h2} is the weight function for two symmetric cracks emanating from a hole in an infinite plate. $W_{collinear}$ used in previous work [4] was limited to $a/t \leq 0.6$. It is extended to $a/t \leq 0.9$ in this work by using Wu and Chen's recent work [5], and is given in Appendix A of this paper.

The solution procedures for surface cracks are exactly the same as those for corner cracks [1], and will not be repeated here. For surface cracks, the following equation gives the relation between stress intensity factors $K(\varphi)$ for a 3-D crack at location φ on the crack front, and the stress intensity factors K_i for the two orthogonal slices intersecting at a common point (x,y) (please refer to Fig. 6 for the definition of crack parameters),

$$K(\varphi) = \frac{(-1)^n}{1-\eta^2(\nu, a/c, \Delta\varphi)} \left\{ K_a^4(a_x) + \left[\frac{E}{E_s} K_c(c_y) \right]^4 \right\}^{\frac{1}{4}} \tag{4}$$

where $n=1$ for $K_i \leq 0$ and $n=2$ for $K_i > 0$. In eq. (4), $\eta(\nu, a/c, \Delta\varphi)$ is a bi-quadratic function of a/c and $\Delta\varphi$ expressed as follows,

$$\eta(\nu, a/c, \Delta\varphi) = \frac{\nu^2}{1+\nu} \left\{ \frac{1}{\nu} + 2\frac{(c/a)}{(c/a)_0} - \frac{(c/a)^2}{(c/a)_0^2} + 2\frac{(\Delta\varphi)}{(\Delta\varphi)_0} - \frac{(\Delta\varphi)^2}{(\Delta\varphi)_0^2} - \frac{(c/a)(\Delta\varphi)}{(c/a)_0(\Delta\varphi)_0} \right\} \tag{5}$$

where ν is Poisson's ratio, $(c/a)_0 = 20$ with $0 \leq c/a \leq 20$, and $(\Delta\varphi)_0 = 10°$ with $0° \leq \Delta\varphi \leq 10°$ measured from the hole surface. For $c/a > 20$ or $\Delta\varphi > 10°$, $\eta = \nu$. The derivation of eq. (5) is given in Appendix B of [1]. The same 3-D finite element solutions for the uncracked stress distribution as in [1] are used.

3. RESULTS AND DISCUSSIONS

The stress intensity factors are given in a dimensionless form defined as

$$F(\varphi)=K(\varphi)/(\sigma_o\sqrt{\pi a}/\Phi) \tag{6}$$

where Φ is the complete elliptic integral of the second kind; σ_0 is a reference stress, $\sigma_0=\sigma_t$ for remote tension, and $\sigma_0=\sigma_w$ for wedge loading in the hole. Some typical crack mouth (x=y=0) displacements are given in the following dimensionless form:

$$COD=\frac{V(0,0)E}{c\sigma_0} \tag{7}$$

3.1 Stress Intensity Factors for Double Surface Cracks

3.1.1 Remote Tension

Tables 1-6 list the weight function results for double surface cracks under remote tension with r/t=0.2, 0.5, 1, 2, 3 and 5, respectively. Comparisons with available finite element solutions [3] are shown in Figs. 7 through 10 for a/c=0.2, 0.4, 2 and 1, respectively. Before discussing the comparison, we note that the finite element solution [3] was obtained for $(c+r)/b\leq 0.2$, while the weight function solution is obtained by using weight functions for (c+r)/b=0, and stress distributions for r/b=0.2. The difference in the models will not cause significant difference between the weight function and the finite element solutions [3], as long as the restraining areas in the finite element model are large enough to resist localized deformation on the front and back surfaces ($y=\pm t$). For the cases of smaller restraining areas, the weight function solutions for infinite width cases will serve as a lower bound of solutions for the cases of finite width.

Inspection of Fig. 7 (a/c=0.2) shows that the agreement between the weight function and the finite element solutions [3] is good away from for the hole surface ($\varphi=90°$), where the precipitous drop-off of the finite element solutions has been shown to be mainly due to some

"ill-shaped" elements around the hole surface [6]. However, the stress intensity factor equation [7], represented by dashed lines in the figure, has good accuracy near the hole surface. The case of r/t=2, a/c=0.2 and a/t=0.8 (Fig. 7 (b)) represents a condition where the restraining areas are the minimum for all the cases compared (r_a=13.5, r_c=72.5, assuming (c+r)/b=0.1 for the finite element model). Since good agreement is observed between the two solutions, it is believed that the weight functions for infinite width plate produces accurate solutions for all the cases with r_a(c/b, r/t, a/c, a/t)$\geq$13.5. (r_c is not important because (c+r)/b is small.) It is also noted that it was for this case that a convergence study of the finite element model was done [8].

For a/c=0.4 (Fig. 8), the agreement is good for $\varphi \leq 45°$. As φ further increases, the two solutions deviate from each other, with the weight function solutions consistently higher than the finite element solutions [3]. For a/c=2 (Fig. 9), the trend is similar to that for a/c=0.4 (Fig. 8), but with a less good agreement for a/t=0.8. The most significant disagreement with [3] is observed for a/c=1 (Fig. 10). Although the agreement near φ=0° is still good, the two solutions have large differences along the rest of the crack front. However, an improved finite element solution for a/t=0.2 and r/b=0.05 by Newman and his colleagues [6] agrees with the weight function result within 5% along most of the crack front. The weight function solution for stress distribution of r/b=0.2 should be 3-4% higher than that for r/b=0.05. Having accounted for this difference, the weight function solution and the improved finite element solution [6] are in excellent agreement.

To further examine the accuracy of the weight function solutions, Figures 11(a,b) and 12 (a,b) compare the weight function results for the limiting cases as a/c$\rightarrow$0 and ∞ to appropriate 2-D solutions, respectively. Figure 11 (a) shows stress intensity factors at φ=90°. It is clear that the stress intensity factor at this point attains the value for 2-D collinear cracks as a/c$\rightarrow$0. Figure 11 (b) shows the variation of stress intensity factors along the crack front; a large value for r/t is used in Fig.11 to keep c/r within the weight function's limit of c/r=2. Similarly, Fig. 12 (a) shows that stress intensity factors at φ=0° approaches the value for through-thickness cracks [9] as a/c$\rightarrow\infty$. Figure 12 (b) shows the variation along the crack front.

Since the 2-D solution [9] is for an infinite width plate, the 2-D stress distribution for r/b=0 is used in the weight function method for this particular comparison.

From the above comparisons and discussions, the large differences observed between some of the weight function and finite element solutions [3] appear to be due to the "ill-shaped" elements [6]. The weight function solutions for surface cracks should have the same degree of accuracy as that for corner cracks [1]. It is noted that the agreement between the weight function and the finite element solutions is much better for surface cracks than for corner cracks [1]. The improved agreement might be attributed to two factors: (a) the enforcement of an additional symmetry condition, and (b) the smaller stress gradients at the center of the plate than at the plate surface, where the surface cracks and the corner cracks are located, respectively. These two factors make it easier for the same finite element model to model the behavior for surface cracks.

3.1.2 **Wedge Loading in the Hole**

This is a load case of practical interest because solutions for this case can be used to obtain solutions for rivet loading by superposition with solutions for remote tension. The wedge loading considered is for a cosine distribution. Tables 7-12 list the weight function solutions for double surface cracks under wedge loading with r/t=0.2, 0.5, 1, 2, 3 and 5, respectively. Since no solutions are available in the literature for this load case, no comparison is made. Figures 13 (a-d) show some typical results for the four different a/c ratios. Typical effect of r/t ratios is shown in Figs. 14 (a, b) for two different crack sizes. Figures 13 and 14 show that (a) the stress intensity factors increase with the hole radius, (b) larger cracks are strongly influenced by variations in hole radius, and (c) very small cracks (small in c/r) are insensitive to changes in hole radius.

It is noted that, per the superposition principle, the stress intensity factors for pin loading, K_p, can be obtained from the results for remote tension, K_t, and wedge loading in the hole, K_w, as follows;

$$K_p = \frac{1}{2}(K_t + K_w) = \sigma_w \sqrt{\pi a}/\Phi \; \frac{1}{2}\left(F_t \frac{r}{b} + F_w\right) = \sigma_w \sqrt{\pi a}/\Phi \; F_p \qquad (8)$$

Equation (8) indicates that for small r/b ratios, F_p is dominated by F_w, while for r/b=0, the value of $F_p = F_w/2$.

3.2 **2-D versus 3-D Uncracked Stress Solutions**

In the literature, applications of weight function methods to cracks emanating from stress concentrations have invariably used uncracked stress distributions from 2-D analysis. As shown for corner cracks [1], in cases of small r/t ratios with small a/t ratios, it is necessary to use 3-D uncracked stress solutions for satisfactory accuracy. Since surface cracks occupy different areas from corner cracks, they may exhibit different behavior. The effect of the stress solutions on the K value is studied for r/b=0.2 under remote tension by comparing results obtained from using 2-D and 3-D uncracked stress distributions. The 2-D uncracked stress distributions are taken from [10]. Figure 15 gives such a comparison for r/t=1.0. Quite different from what observed for corner cracks [1], the differences caused by 2-D and 3-D uncracked stress distributions are negligibly small. Therefore, 2-D uncracked stress distributions can be used to obtain solutions with reasonable accuracy.

3.3 **Single Crack**

A single surface crack can be considered by using appropriate weight functions for c-slices. Grandt [2] obtained solutions for a single surface crack by using a 3-D finite element alternating method. We compare his solutions for remote tension with weight function results. To be identical, the Poisson's ratio is assumed as 0.25 in the weight function method. Figure 16 compares all the solutions available, except for a/t=1, which is beyond the weight function range of $a/t \leq 0.9$. It can be seen that the agreement is very good at $\varphi = 30°$ and 60°, but with significant differences around $\varphi = 90°$. The reason why the finite element alternating solutions [2] are low at surface is unknown. It is believed that the weight function results are accurate,

as evidenced by the excellent agreement between weight function predictions and improved finite element analysis [6] (Fig.10(a)).

3.4 Difference between Single and Double Cracks

As mentioned in [1], Shah's conversion factor [11] is invariably used in the literature to obtain stress intensity factors for single crack by using solutions for double cracks, or vice versa. We examine the actual difference between single and double surface cracks. Figures 17 (a) and (b) show the differences between single and double cracks for three typical crack shapes under the same L/r ratio of 1.005, where L is the length of a through-thickness crack that has the same area as a surface crack. Because of the large a/t and small r/t ratios considered, the differences observed in Fig. 17 are among the largest that surface cracks could have for the load case. Figure 17 (c) compares the ratio K_d/K_s, where K_d is for double cracks and K_s for a single crack. Similarly to corner cracks [1], the ratio of K_d/K_s increases with a/c, since the surface crack becomes closer to a through crack. Also shown in Fig. 17 (c) are the results from Shah's conversion factor [11], and from through-thickness cracks [12]. In these cases, Shah's results have an error in the range of 4-13% and will overestimate K_d or underestimate K_s, depending upon which one is the known solution. For very small cracks (small in c/r), single crack and double cracks will have the same solution.

3.5 Crack Face Displacements

Crack face displacement is a useful parameter in fatigue and fracture experiments, in fatigue crack modeling and in fracture criterion. Parallel with the work for corner cracks [1], some typical crack face displacements at the crack mouth location (x=y=0) are shown in Fig. 18. A large range of a/c ratios from 1 to 80 is considered, as represented by circles in the Figure. Also shown in Fig. 18 is the result for through-thickness cracks by Mall and Newman [9], with plane strain conditions assumed. As can be seen, the crack face displacement for surface cracks approaches that for through-thickness cracks as a/c increases (c/r decreases as a consequence). A small difference (3%) at a/c=80 (c/r=0.005) is due to inaccuracies in the

weight function; crack face displacements at other locations are expected to have better accuracy than at the crack mouth.

4. CONCLUDING REMARKS

Detailed analysis of surface cracks emanating from a circular hole has been performed for two different loading conditions: remote tension and wedge loading in the hole. A wide range in configuration parameters is considered. They are r/t=0.2, 0.5, 1, 2, 3 and 5; a/c=0.2, 0.4, 1 and 2; and a/t=0.01, 0.1, 0.2, 0.3, 0.4, 0.5, 0.6, 0.7, 0.8 and 0.9 within the limit of c/r=2. The accuracy and efficiency of the 3-D weight function method is further demonstrated. The study shows that unlike the case for corner cracks, the 2-D uncracked stress distribution can be used with satisfactory accuracy in the range considered, because the difference in the uncracked stress distribution between 2-D and 3-D solutions is small in the center region of a plate, where the surface cracks are located. The difference in stress intensity factors between single and double surface cracks is investigated, which reveals that if Shah's conversion factor [11] is used, an error of 4-13% will be involved in estimating stress intensity factors. Typical crack face displacements are also presented. This work provides extensive solutions for practical damage tolerance analysis, especially for the wedge loading case, for which no solutions were available in the literature previously.

REFERENCES

[1] W. Zhao, J.C. Newman, Jr., M.A. Sutton, X.R. Wu and K.N. Shivakumar, Analysis of corner cracks at hole by a 3-D weight function method with stresses from finite element analysis. NASA TM-110144 (1995).

[2] A.F. Grandt, Jr., Crack face pressure loading of semielliptical cracks located along the bore of a hole. Engng. Fracture Mech. 14, 843-852 (1981).

[3] J.C. Newman Jr.and I.S. Raju, Stress intensity factor equations for cracks in three-dimensional finite bodies. ASTM STP 791,(Edited by J.C. Lewis and G. Sines), I-238 - I-256 (1983).

[4] W. Zhao, X.R. Wu and M.G. Yan, Weight function method for three dimensional crack problems-II. Engng. Fracture Mech. 34, 609-624 (1989).

[5] X.R. Wu and X.G Chen, Wide-range weight function for center cracks. Engng. Fracture Mech. 33, 877-886 (1989).

[6] P.W. Tan, I.S. Raju, K.N. Shivakumar and J.C. Newman, Jr., Evaluation of finite element models and stress intensity factors for surface cracks emanating from stress concentrations. ASTM STP 1060, W.G. Reuter, J.H. Underwood and J.C. Newman, Jr., Eds., 34-48 (1990).

[7] J.C Newman, Jr. and I.S. Raju, Stress intensity factor equations for cracks in three-dimensional finite bodies subjected to tension and bending loads. in Computational methods in the mechanics of fracture. (Edited by S.N. Atluri) 312-334 (1986).

[8] I.S. Raju and J.C. Newman, Jr., Stress intensity factors for two symmetric corner cracks. ASTM STP 677, C.W. Smith, Ed., 411-430 (1979).

[9] S. Mall and J.C. Newman, Jr., Crack-surface displacements for two symmetric cracks emanating from a circular hole in an infinite plate. Engng. Fracture Mech. 24, 929-931 (1986).

[10] R.C. Howland, On the stresses in the neighborhood of a circular hole in a strip under tension. Phil. Trans. Roy. Soc. London, A, 229, 49 (1930).

[11] R.C. Shah, Stress intensity factors for through and part-through cracks originating at a fastener holes. ASTM STP 590, 429-459 (1976).

[12] X.R.Wu and J.Carlsson, Weight functions and stress intensity factor solutions. Pergamon press, (1991).

Appendix A

The weight function $W_{collinear}$ in eq. (3a) is taken from Wu and Chen [5]. It was developed by making an assumed symmetric crack face displacement expression satisfy the following two conditions: (i) K-controlled near-tip crack face displacement, (ii) self-consistent K factor. The resulting weight function has an accuracy better than 2% in K for $a/t \leq 0.85$.

Defining the dimensionless crack length $s=a/t$, and the coordinate $\xi=y/t$, the weight function [5] is expressed as follows:

$$W_{collinear}(s,\xi)=\frac{1}{\sqrt{\pi a}\,f(s)}\sum_{i=1}^{3}\beta_i(s)(s^2-\xi^2)^{i-\frac{3}{2}} \qquad \text{(A1)}$$

where f(s) is a dimensionless reference stress intensity factor (as in $K=\sigma(\pi a)^{1/2}f(s)$), and

$$\beta_1 = 2sf(s)$$
$$\beta_2 = 3G(s)/s + 2f'(s) \qquad \text{(A2)}$$
$$\beta_3 = [G'(s) - 2G(s)/s]/s^2$$

where "′" represents differentiation with respect to s, and

$$G(s) = \frac{16}{3}[\Phi(s) - f(s)/2]$$
$$\Phi(s) = \frac{1}{s^2}\int_0^s \zeta f^2(\zeta)\, d\zeta \qquad \text{(A3)}$$

The reference load case used is a uniform crack face pressure, σ.

Table 1 Dimensionless stress intensity factors for double surface cracks at a hole under remote tension, r/t=0.2

a/c	a/t	$\varphi°$ 0.1	11.3	22.5	33.8	45.0	56.3	67.5	82.5	89.9
0.2	0.01	0.909	1.079	1.364	1.641	1.908	2.177	2.456	2.864	3.078
0.4	0.01	1.558	1.641	1.838	2.064	2.296	2.531	2.759	3.083	3.274
1.0	0.01	2.823	2.834	2.869	2.901	2.935	3.001	3.089	3.285	3.471
	0.1	1.738	1.752	1.780	1.837	1.930	2.059	2.242	2.648	2.956
	0.2	1.422	1.433	1.440	1.481	1.564	1.667	1.833	2.280	2.690
2.0	0.01	2.150	2.140	2.114	2.052	1.963	1.873	1.784	1.750	1.868
	0.1	1.561	1.557	1.550	1.534	1.510	1.487	1.469	1.529	1.669
	0.2	1.277	1.272	1.264	1.258	1.254	1.250	1.259	1.375	1.539
	0.3	1.135	1.128	1.117	1.113	1.115	1.113	1.128	1.271	1.457
	0.4	1.053	1.045	1.030	1.027	1.031	1.027	1.041	1.193	1.399

Table 2 Dimensionless stress intensity factors for double surface cracks at a hole under remote tension, r/t=0.5

a/c	a/t	$\varphi°$ 0.1	11.3	22.5	33.8	45.0	56.3	67.5	82.5	89.9
0.2	0.01	1.159	1.371	1.724	2.047	2.334	2.598	2.839	3.142	3.288
	0.1	0.597	0.716	0.891	1.078	1.274	1.484	1.750	2.349	2.830
0.4	0.01	1.799	1.888	2.107	2.349	2.578	2.796	2.992	3.239	3.351
	0.1	1.067	1.132	1.270	1.451	1.662	1.902	2.190	2.701	3.005
	0.2	0.859	0.918	1.016	1.158	1.329	1.525	1.785	2.355	2.804
1.0	0.01	3.071	3.081	3.112	3.134	3.152	3.202	3.272	3.448	3.629
	0.1	2.330	2.345	2.388	2.447	2.527	2.647	2.802	3.110	3.347
	0.2	1.918	1.933	1.968	2.031	2.128	2.266	2.454	2.849	3.143
	0.3	1.696	1.710	1.736	1.795	1.895	2.031	2.226	2.669	3.012
	0.4	1.565	1.578	1.597	1.653	1.752	1.880	2.071	2.539	2.927
	0.5	1.484	1.496	1.510	1.564	1.662	1.782	1.969	2.451	2.882
2.0	0.01	2.277	2.266	2.235	2.165	2.065	1.964	1.865	1.821	1.941
	0.1	1.951	1.945	1.929	1.889	1.829	1.769	1.710	1.714	1.843
	0.2	1.704	1.699	1.690	1.668	1.635	1.604	1.575	1.621	1.760
	0.3	1.535	1.531	1.525	1.513	1.496	1.481	1.472	1.550	1.700
	0.4	1.417	1.413	1.407	1.401	1.394	1.388	1.391	1.494	1.655
	0.5	1.333	1.328	1.322	1.320	1.319	1.318	1.330	1.454	1.626
	0.6	1.273	1.267	1.260	1.261	1.265	1.268	1.288	1.430	1.614
	0.7	1.229	1.223	1.216	1.220	1.230	1.237	1.262	1.419	1.617
	0.8	1.200	1.193	1.186	1.194	1.211	1.221	1.252	1.428	1.644
	0.9	1.182	1.175	1.169	1.186	1.213	1.229	1.277	1.489	1.733

Table 3 Dimensionless stress intensity factors for double surface cracks at a hole under remote tension, r/t=1.0

a/c	a/t	$\varphi°$ 0.1	11.3	22.5	33.8	45.0	56.3	67.5	82.5	89.9
0.2	0.01	1.263	1.491	1.869	2.203	2.487	2.734	2.946	3.195	3.312
	0.1	0.746	0.889	1.122	1.360	1.602	1.864	2.166	2.692	3.010
	0.2	0.598	0.718	0.893	1.081	1.280	1.493	1.763	2.362	2.837
0.4	0.01	1.878	1.969	2.192	2.434	2.657	2.862	3.041	3.259	3.356
	0.1	1.334	1.407	1.583	1.797	2.030	2.280	2.548	2.951	3.154
	0.2	1.070	1.135	1.273	1.456	1.668	1.911	2.201	2.712	3.012
	0.3	0.940	1.001	1.117	1.279	1.474	1.699	1.985	2.549	2.931
	0.4	0.869	0.928	1.031	1.180	1.364	1.572	1.847	2.434	2.887
1.0	0.01	3.111	3.120	3.148	3.166	3.178	3.221	3.283	3.447	3.625
	0.1	2.668	2.682	2.722	2.766	2.821	2.911	3.027	3.267	3.473
	0.2	2.330	2.345	2.388	2.447	2.528	2.649	2.805	3.112	3.349
	0.3	2.099	2.115	2.156	2.222	2.319	2.457	2.637	2.998	3.265
	0.4	1.939	1.954	1.993	2.062	2.168	2.313	2.508	2.911	3.208
	0.5	1.827	1.841	1.877	1.948	2.059	2.208	2.414	2.855	3.182
	0.6	1.748	1.762	1.796	1.868	1.984	2.140	2.359	2.836	3.195
	0.7	1.695	1.709	1.742	1.818	1.943	2.109	2.345	2.856	3.250
	0.8	1.664	1.680	1.713	1.796	1.937	2.120	2.379	2.947	3.391
	0.9	1.657	1.674	1.708	1.808	1.980	2.197	2.527	3.238	3.772
2.0	0.01	2.284	2.273	2.241	2.169	2.067	1.964	1.862	1.816	1.934
	0.1	2.108	2.099	2.076	2.021	1.942	1.861	1.782	1.761	1.883
	0.2	1.947	1.940	1.924	1.884	1.824	1.765	1.707	1.711	1.839
	0.3	1.818	1.813	1.801	1.773	1.729	1.686	1.645	1.672	1.806
	0.4	1.715	1.711	1.702	1.682	1.651	1.620	1.592	1.640	1.780
	0.5	1.633	1.628	1.623	1.609	1.587	1.566	1.550	1.617	1.765
	0.6	1.568	1.563	1.559	1.550	1.537	1.525	1.521	1.607	1.763
	0.7	1.517	1.513	1.510	1.506	1.502	1.498	1.505	1.609	1.776
	0.8	1.480	1.476	1.474	1.477	1.482	1.487	1.506	1.637	1.819
	0.9	1.455	1.452	1.451	1.464	1.485	1.505	1.551	1.740	1.952

Table 4 Dimensionless stress intensity factors for double surface cracks at a hole under remote tension, r/t=2.0

a/c	a/t	$\varphi°$ 0.1	11.3	22.5	33.8	45.0	56.3	67.5	82.5	89.9
0.2	0.01	1.304	1.539	1.925	2.260	2.537	2.772	2.965	3.183	3.284
	0.1	0.918	1.090	1.378	1.658	1.928	2.200	2.482	2.894	3.109
	0.2	0.734	0.875	1.105	1.339	1.581	1.841	2.143	2.668	2.987
	0.3	0.645	0.772	0.968	1.177	1.397	1.637	1.932	2.516	2.923
	0.4	0.596	0.716	0.893	1.088	1.296	1.519	1.798	2.411	2.895
0.4	0.01	1.895	1.986	2.209	2.448	2.664	2.861	3.028	3.229	3.319
	0.1	1.551	1.631	1.829	2.058	2.289	2.523	2.753	3.065	3.211
	0.2	1.312	1.385	1.558	1.770	2.002	2.253	2.522	2.926	3.130
	0.3	1.161	1.229	1.383	1.582	1.810	2.066	2.358	2.832	3.089
	0.4	1.063	1.127	1.268	1.458	1.681	1.937	2.240	2.768	3.076
	0.5	0.997	1.060	1.192	1.375	1.596	1.850	2.164	2.740	3.099
	0.6	0.952	1.016	1.142	1.323	1.545	1.805	2.136	2.762	3.172
	0.7	0.924	0.989	1.112	1.295	1.526	1.804	2.161	2.844	3.310
	0.8	0.910	0.977	1.100	1.292	1.544	1.852	2.256	3.037	3.582
1.0	0.01	3.092	3.100	3.128	3.143	3.151	3.190	3.248	3.405	3.578
	0.1	2.850	2.861	2.895	2.927	2.961	3.028	3.116	3.314	3.502
	0.2	2.629	2.642	2.682	2.727	2.784	2.876	2.994	3.236	3.441
	0.3	2.453	2.468	2.511	2.569	2.644	2.758	2.901	3.183	3.407
	0.4	2.315	2.330	2.377	2.444	2.535	2.665	2.829	3.149	3.391
	0.5	2.206	2.223	2.271	2.346	2.450	2.595	2.780	3.139	3.403
	0.6	2.123	2.140	2.191	2.273	2.390	2.553	2.765	3.168	3.456
	0.7	2.062	2.080	2.134	2.225	2.359	2.547	2.790	3.243	3.560
	0.8	2.023	2.044	2.100	2.204	2.364	2.585	2.871	3.408	3.770
	0.9	2.010	2.034	2.094	2.220	2.424	2.701	3.090	3.829	4.286
2.0	0.01	2.260	2.248	2.216	2.145	2.042	1.939	1.838	1.791	1.907
	0.1	2.169	2.159	2.132	2.069	1.979	1.888	1.798	1.764	1.882
	0.2	2.077	2.069	2.046	1.993	1.915	1.837	1.760	1.740	1.862
	0.3	1.998	1.991	1.973	1.928	1.863	1.796	1.731	1.725	1.851
	0.4	1.931	1.925	1.911	1.874	1.819	1.762	1.707	1.714	1.844
	0.5	1.875	1.869	1.858	1.828	1.782	1.735	1.690	1.712	1.848
	0.6	1.828	1.822	1.814	1.791	1.755	1.718	1.685	1.724	1.866
	0.7	1.790	1.785	1.781	1.765	1.739	1.715	1.696	1.752	1.903
	0.8	1.762	1.759	1.757	1.750	1.738	1.729	1.726	1.812	1.979
	0.9	1.745	1.744	1.745	1.753	1.764	1.778	1.812	1.969	2.170

Table 5 Dimensionless stress intensity factors for double surface cracks at a hole under remote tension, r/t=3.0

a/c	a/t	$\varphi°$ 0.1	11.3	22.5	33.8	45.0	56.3	67.5	82.5	89.9
0.2	0.01	1.312	1.547	1.934	2.268	2.541	2.770	2.955	3.161	3.257
	0.1	1.013	1.200	1.515	1.811	2.086	2.351	2.610	2.961	3.136
	0.2	0.834	0.991	1.253	1.514	1.773	2.045	2.339	2.797	3.049
	0.3	0.732	0.872	1.101	1.338	1.583	1.848	2.155	2.686	3.007
	0.4	0.670	0.801	1.008	1.231	1.466	1.722	2.030	2.611	2.996
	0.5	0.631	0.756	0.950	1.165	1.394	1.644	1.953	2.577	3.023
	0.6	0.606	0.729	0.915	1.126	1.355	1.609	1.927	2.595	3.103
0.4	0.01	1.891	1.981	2.202	2.439	2.652	2.844	3.007	3.201	3.287
	0.1	1.642	1.726	1.930	2.161	2.388	2.610	2.819	3.092	3.217
	0.2	1.445	1.521	1.709	1.931	2.164	2.407	2.654	3.001	3.167
	0.3	1.304	1.376	1.549	1.765	2.001	2.258	2.533	2.945	3.151
	0.4	1.202	1.272	1.434	1.645	1.884	2.150	2.447	2.914	3.160
	0.5	1.129	1.197	1.352	1.559	1.801	2.076	2.394	2.917	3.203
	0.6	1.077	1.144	1.294	1.501	1.748	2.038	2.385	2.972	3.302
	0.7	1.041	1.108	1.257	1.467	1.728	2.043	2.430	3.092	3.471
	0.8	1.019	1.090	1.238	1.458	1.745	2.101	2.548	3.335	3.789
	0.9	1.013	1.091	1.240	1.480	1.816	2.247	2.843	3.940	4.540
1.0	0.01	3.069	3.077	3.103	3.117	3.125	3.162	3.218	3.372	3.543
	0.1	2.904	2.914	2.946	2.972	2.997	3.054	3.131	3.313	3.494
	0.2	2.744	2.756	2.793	2.830	2.874	2.952	3.052	3.266	3.459
	0.3	2.611	2.625	2.666	2.715	2.777	2.875	2.997	3.243	3.450
	0.4	2.501	2.516	2.562	2.623	2.701	2.816	2.958	3.236	3.458
	0.5	2.412	2.428	2.479	2.550	2.642	2.775	2.940	3.254	3.494
	0.6	2.342	2.359	2.414	2.495	2.605	2.760	2.955	3.314	3.575
	0.7	2.289	2.308	2.369	2.463	2.594	2.780	3.013	3.424	3.711
	0.8	2.256	2.279	2.345	2.456	2.618	2.846	3.130	3.633	3.966
	0.9	2.249	2.276	2.348	2.486	2.701	2.997	3.402	4.129	4.561
0.2	0.01	2.239	2.227	2.196	2.124	2.023	1.920	1.819	1.773	1.888
	0.1	2.178	2.168	2.140	2.074	1.981	1.886	1.793	1.755	1.872
	0.2	2.116	2.107	2.082	2.023	1.939	1.854	1.770	1.742	1.861
	0.3	2.062	2.054	2.032	1.981	1.906	1.830	1.755	1.737	1.859
	0.4	2.015	2.008	1.990	1.946	1.880	1.812	1.745	1.737	1.863
	0.5	1.976	1.969	1.955	1.917	1.859	1.800	1.741	1.746	1.876
	0.6	1.944	1.938	1.927	1.896	1.847	1.798	1.751	1.770	1.907
	0.7	1.919	1.914	1.907	1.883	1.846	1.810	1.776	1.811	1.957
	0.8	1.903	1.900	1.897	1.883	1.861	1.841	1.824	1.889	2.051
	0.9	1.898	1.896	1.898	1.900	1.903	1.910	1.934	2.074	2.272

Table 6 Dimensionless stress intensity factors for double surface cracks at a hole under remote tension, r/t=5.0

a/c	a/t	φ° 0.1	11.3	22.5	33.8	45.0	56.3	67.5	82.5	89.9
0.2	0.01	1.319	1.554	1.942	2.274	2.544	2.767	2.946	3.142	3.234
	0.1	1.114	1.318	1.658	1.968	2.244	2.498	2.730	3.021	3.162
	0.2	0.962	1.140	1.441	1.728	2.002	2.272	2.543	2.921	3.112
	0.3	0.859	1.020	1.292	1.563	1.832	2.112	2.410	2.859	3.099
	0.4	0.788	0.938	1.189	1.448	1.715	1.999	2.316	2.826	3.113
	0.5	0.738	0.881	1.117	1.370	1.635	1.924	2.259	2.828	3.164
	0.6	0.703	0.841	1.069	1.318	1.587	1.888	2.249	2.884	3.272
	0.7	0.680	0.816	1.038	1.289	1.569	1.895	2.294	3.010	3.456
	0.8	0.666	0.802	1.023	1.283	1.589	1.955	2.414	3.264	3.796
	0.9	0.662	0.803	1.025	1.304	1.659	2.101	2.712	3.897	4.597
0.4	0.01	1.898	1.992	2.215	2.449	2.664	2.864	3.034	3.256	3.398
	0.1	1.745	1.834	2.047	2.278	2.502	2.719	2.915	3.179	3.340
	0.2	1.607	1.691	1.893	2.121	2.353	2.586	2.808	3.116	3.299
	0.3	1.498	1.578	1.771	1.998	2.238	2.486	2.732	3.083	3.287
	0.4	1.412	1.489	1.676	1.903	2.150	2.411	2.678	3.070	3.297
	0.5	1.345	1.420	1.602	1.831	2.085	2.359	2.649	3.086	3.339
	0.6	1.294	1.368	1.547	1.779	2.043	2.337	2.658	3.150	3.432
	0.7	1.258	1.331	1.510	1.748	2.028	2.353	2.715	3.272	3.589
	0.8	1.235	1.310	1.490	1.740	2.049	2.417	2.838	3.506	3.879
	0.9	1.230	1.309	1.492	1.765	2.125	2.568	3.129	4.065	4.556
1.0	0.01	3.113	3.121	3.146	3.155	3.167	3.209	3.266	3.454	3.697
	0.1	3.013	3.022	3.050	3.067	3.088	3.142	3.211	3.414	3.661
	0.2	2.911	2.921	2.952	2.977	3.011	3.079	3.162	3.384	3.637
	0.3	2.822	2.833	2.868	2.903	2.951	3.032	3.130	3.372	3.633
	0.4	2.747	2.759	2.798	2.843	2.903	2.997	3.109	3.372	3.642
	0.5	2.684	2.697	2.740	2.794	2.867	2.974	3.104	3.393	3.674
	0.6	2.633	2.647	2.695	2.759	2.845	2.972	3.126	3.446	3.743
	0.7	2.595	2.609	2.663	2.739	2.844	2.997	3.182	3.541	3.856
	0.8	2.570	2.587	2.647	2.738	2.871	3.059	3.285	3.714	4.066
	0.9	2.563	2.582	2.649	2.767	2.947	3.191	3.517	4.117	4.549
2.0	0.01	2.221	2.210	2.178	2.107	2.006	1.904	1.804	1.757	1.871
	0.1	2.186	2.176	2.146	2.078	1.982	1.885	1.789	1.748	1.863
	0.2	2.149	2.139	2.112	2.049	1.959	1.868	1.779	1.744	1.860
	0.3	2.118	2.109	2.084	2.026	1.943	1.859	1.776	1.748	1.867
	0.4	2.092	2.083	2.062	2.010	1.934	1.855	1.778	1.757	1.879
	0.5	2.071	2.063	2.045	1.999	1.929	1.858	1.787	1.776	1.903
	0.6	2.057	2.049	2.034	1.994	1.933	1.871	1.810	1.811	1.944
	0.7	2.048	2.042	2.031	1.998	1.948	1.899	1.851	1.866	2.008
	0.8	2.047	2.043	2.037	2.014	1.980	1.948	1.916	1.961	2.119
	0.9	2.057	2.055	2.054	2.049	2.042	2.037	2.049	2.171	2.368

Table 7 Dimensionless stress intensity factors for double surface cracks at a hole under wedge loading, r/t=0.2

a/c	a/t	$\varphi°$ 0.1	11.3	22.5	33.8	45.0	56.3	67.5	82.5	89.9
0.2	0.01	0.365	0.435	0.555	0.680	0.812	0.959	1.130	1.423	1.598
0.4	0.01	0.707	0.746	0.841	0.955	1.080	1.216	1.360	1.581	1.712
1.0	0.01	1.403	1.410	1.432	1.456	1.485	1.534	1.597	1.726	1.837
	0.1	0.625	0.634	0.651	0.688	0.752	0.836	0.957	1.239	1.476
	0.2	0.386	0.394	0.401	0.433	0.495	0.570	0.688	0.978	1.297
2.0	0.01	1.110	1.106	1.094	1.065	1.023	0.981	0.939	0.929	0.994
	0.1	0.664	0.663	0.664	0.667	0.670	0.676	0.689	0.759	0.853
	0.2	0.476	0.475	0.476	0.485	0.501	0.518	0.546	0.648	0.768
	0.3	0.374	0.372	0.373	0.385	0.406	0.426	0.460	0.573	0.715
	0.4	0.308	0.305	0.305	0.319	0.343	0.364	0.401	0.516	0.675

Table 8 Dimensionless stress intensity factors for double surface cracks at a hole under wedge loading, r/t=0.5

a/c	a/t	$\varphi°$ 0.1	11.3	22.5	33.8	45.0	56.3	67.5	82.5	89.9
0.2	0.01	0.533	0.632	0.800	0.961	1.114	1.265	1.418	1.629	1.727
	0.1	0.132	0.168	0.212	0.278	0.362	0.473	0.638	1.028	1.426
0.4	0.01	0.892	0.938	1.051	1.179	1.306	1.433	1.554	1.715	1.790
	0.1	0.368	0.396	0.449	0.530	0.634	0.762	0.931	1.278	1.532
	0.2	0.209	0.233	0.260	0.316	0.398	0.504	0.662	1.020	1.382
1.0	0.01	1.603	1.609	1.628	1.643	1.659	1.693	1.738	1.843	1.946
	0.1	1.016	1.025	1.050	1.090	1.148	1.232	1.343	1.569	1.735
	0.2	0.741	0.751	0.771	0.811	0.876	0.965	1.090	1.369	1.589
	0.3	0.587	0.596	0.611	0.651	0.718	0.805	0.932	1.229	1.492
	0.4	0.485	0.494	0.506	0.544	0.613	0.697	0.825	1.125	1.425
	0.5	0.414	0.422	0.432	0.469	0.537	0.619	0.748	1.051	1.382
2.0	0.01	1.209	1.203	1.188	1.152	1.101	1.049	0.998	0.978	1.043
	0.1	0.933	0.932	0.928	0.916	0.898	0.881	0.866	0.891	0.969
	0.2	0.756	0.755	0.755	0.754	0.752	0.753	0.759	0.818	0.909
	0.3	0.642	0.641	0.643	0.647	0.654	0.663	0.680	0.761	0.864
	0.4	0.563	0.562	0.564	0.572	0.584	0.598	0.622	0.717	0.830
	0.5	0.505	0.503	0.505	0.516	0.532	0.549	0.578	0.683	0.807
	0.6	0.460	0.458	0.460	0.472	0.493	0.513	0.547	0.660	0.796
	0.7	0.424	0.422	0.424	0.439	0.463	0.486	0.524	0.644	0.793
	0.8	0.396	0.393	0.396	0.413	0.440	0.465	0.508	0.635	0.800
	0.9	0.375	0.371	0.374	0.395	0.427	0.454	0.505	0.642	0.829

Table 9 Dimensionless stress intensity factors for double surface cracks at a hole under wedge loading, r/t=1.0

a/c	a/t	$\varphi°$ 0.1	11.3	22.5	33.8	45.0	56.3	67.5	82.5	89.9
0.2	0.01	0.628	0.742	0.933	1.109	1.263	1.404	1.533	1.691	1.758
	0.1	0.252	0.305	0.391	0.491	0.606	0.744	0.925	1.293	1.563
	0.2	0.136	0.172	0.219	0.286	0.372	0.486	0.655	1.048	1.441
0.4	0.01	0.975	1.023	1.142	1.273	1.396	1.513	1.619	1.752	1.812
	0.1	0.555	0.589	0.667	0.770	0.891	1.032	1.199	1.488	1.654
	0.2	0.377	0.405	0.460	0.542	0.648	0.779	0.950	1.296	1.546
	0.3	0.279	0.305	0.345	0.414	0.510	0.631	0.800	1.164	1.477
	0.4	0.218	0.242	0.272	0.331	0.419	0.531	0.697	1.068	1.431
1.0	0.01	1.660	1.665	1.682	1.694	1.703	1.730	1.768	1.862	1.960
	0.1	1.277	1.285	1.311	1.344	1.388	1.455	1.541	1.710	1.842
	0.2	1.030	1.040	1.065	1.105	1.163	1.247	1.358	1.583	1.747
	0.3	0.874	0.883	0.906	0.949	1.014	1.104	1.227	1.487	1.681
	0.4	0.764	0.773	0.795	0.838	0.907	1.000	1.129	1.411	1.632
	0.5	0.682	0.692	0.711	0.756	0.827	0.921	1.055	1.356	1.603
	0.6	0.620	0.629	0.647	0.692	0.767	0.863	1.003	1.320	1.594
	0.7	0.572	0.580	0.598	0.644	0.722	0.822	0.971	1.303	1.605
	0.8	0.535	0.544	0.561	0.609	0.693	0.799	0.960	1.314	1.653
	0.9	0.510	0.518	0.535	0.590	0.685	0.801	0.992	1.403	1.801
2.0	0.01	1.230	1.224	1.207	1.169	1.115	1.060	1.006	0.983	1.047
	0.1	1.071	1.068	1.059	1.036	1.002	0.969	0.936	0.937	1.008
	0.2	0.941	0.939	0.935	0.923	0.904	0.886	0.871	0.895	0.973
	0.3	0.845	0.844	0.842	0.837	0.828	0.822	0.818	0.861	0.946
	0.4	0.771	0.770	0.771	0.770	0.768	0.769	0.775	0.833	0.925
	0.5	0.713	0.712	0.714	0.717	0.720	0.726	0.739	0.812	0.910
	0.6	0.667	0.666	0.668	0.674	0.682	0.693	0.713	0.798	0.904
	0.7	0.631	0.629	0.632	0.640	0.653	0.668	0.694	0.790	0.905
	0.8	0.601	0.600	0.603	0.614	0.632	0.651	0.683	0.793	0.919
	0.9	0.578	0.577	0.581	0.597	0.622	0.646	0.689	0.827	0.971

Table 10 Dimensionless stress intensity factors for double surface cracks at a hole under wedge loading, r/t=2.0

a/c	a/t	$\varphi°$ 0.1	11.3	22.5	33.8	45.0	56.3	67.5	82.5	89.9
0.2	0.01	0.678	0.799	1.002	1.182	1.334	1.465	1.577	1.704	1.755
	0.1	0.373	0.445	0.568	0.697	0.833	0.984	1.162	1.465	1.638
	0.2	0.246	0.298	0.382	0.480	0.595	0.733	0.915	1.286	1.557
	0.3	0.177	0.219	0.280	0.360	0.460	0.587	0.766	1.162	1.507
	0.4	0.134	0.170	0.216	0.284	0.373	0.490	0.665	1.072	1.475
0.4	0.01	1.009	1.058	1.178	1.308	1.428	1.538	1.634	1.751	1.803
	0.1	0.714	0.753	0.850	0.967	1.095	1.233	1.381	1.603	1.715
	0.2	0.545	0.579	0.656	0.758	0.879	1.021	1.190	1.481	1.648
	0.3	0.443	0.473	0.537	0.629	0.744	0.884	1.060	1.392	1.606
	0.4	0.372	0.400	0.455	0.540	0.650	0.787	0.966	1.325	1.581
	0.5	0.320	0.347	0.396	0.475	0.582	0.716	0.899	1.279	1.575
	0.6	0.282	0.308	0.350	0.426	0.531	0.666	0.856	1.257	1.593
	0.7	0.252	0.278	0.317	0.390	0.496	0.635	0.837	1.263	1.640
	0.8	0.231	0.257	0.292	0.365	0.476	0.624	0.846	1.313	1.745
1.0	0.01	1.671	1.675	1.691	1.700	1.706	1.729	1.763	1.851	1.946
	0.1	1.445	1.452	1.475	1.499	1.528	1.577	1.640	1.771	1.884
	0.2	1.262	1.270	1.296	1.329	1.374	1.443	1.530	1.700	1.832
	0.3	1.127	1.136	1.163	1.203	1.258	1.339	1.443	1.647	1.797
	0.4	1.025	1.035	1.062	1.106	1.169	1.258	1.374	1.605	1.773
	0.5	0.947	0.956	0.983	1.030	1.099	1.194	1.321	1.579	1.765
	0.6	0.885	0.894	0.922	0.971	1.046	1.148	1.287	1.572	1.779
	0.7	0.836	0.846	0.874	0.927	1.008	1.121	1.274	1.586	1.816
	0.8	0.800	0.811	0.839	0.897	0.989	1.114	1.287	1.640	1.902
	0.9	0.777	0.788	0.817	0.885	0.995	1.143	1.360	1.809	2.127
2.0	0.01	1.226	1.220	1.203	1.164	1.110	1.054	0.999	0.975	1.038
	0.1	1.141	1.136	1.124	1.094	1.050	1.006	0.963	0.951	1.018
	0.2	1.060	1.056	1.048	1.026	0.992	0.960	0.928	0.930	1.001
	0.3	0.993	0.990	0.985	0.969	0.945	0.921	0.899	0.914	0.988
	0.4	0.937	0.935	0.932	0.921	0.904	0.888	0.874	0.900	0.979
	0.5	0.891	0.889	0.888	0.882	0.870	0.860	0.854	0.892	0.975
	0.6	0.852	0.851	0.851	0.848	0.843	0.839	0.841	0.890	0.980
	0.7	0.821	0.820	0.821	0.822	0.822	0.826	0.835	0.897	0.992
	0.8	0.796	0.795	0.798	0.803	0.810	0.821	0.838	0.918	1.024
	0.9	0.777	0.777	0.781	0.793	0.811	0.832	0.867	0.983	1.108

Table 11 Dimensionless stress intensity factors for double surface cracks at a hole under wedge loading, r/t=3.0

a/c	a/t	$\varphi°$ 0.1	11.3	22.5	33.8	45.0	56.3	67.5	82.5	89.9
0.2	0.01	0.692	0.815	1.020	1.200	1.349	1.475	1.580	1.695	1.740
	0.1	0.440	0.523	0.665	0.808	0.952	1.104	1.270	1.526	1.658
	0.2	0.315	0.379	0.484	0.599	0.726	0.874	1.056	1.390	1.600
	0.3	0.243	0.295	0.378	0.477	0.592	0.733	0.917	1.293	1.568
	0.4	0.195	0.240	0.307	0.395	0.502	0.636	0.821	1.221	1.551
	0.5	0.161	0.201	0.257	0.336	0.437	0.567	0.754	1.173	1.553
	0.6	0.136	0.173	0.221	0.294	0.390	0.518	0.712	1.151	1.581
0.4	0.01	1.013	1.062	1.182	1.311	1.428	1.534	1.626	1.737	1.786
	0.1	0.789	0.831	0.935	1.056	1.183	1.315	1.448	1.636	1.727
	0.2	0.638	0.675	0.763	0.875	1.000	1.142	1.301	1.550	1.681
	0.3	0.540	0.573	0.650	0.753	0.877	1.021	1.194	1.489	1.658
	0.4	0.469	0.501	0.570	0.667	0.788	0.933	1.114	1.444	1.648
	0.5	0.417	0.447	0.509	0.603	0.722	0.869	1.057	1.417	1.656
	0.6	0.376	0.405	0.463	0.554	0.674	0.824	1.024	1.416	1.690
	0.7	0.344	0.373	0.428	0.518	0.641	0.801	1.017	1.444	1.756
	0.8	0.320	0.350	0.402	0.493	0.625	0.799	1.042	1.525	1.889
	0.9	0.304	0.336	0.385	0.482	0.631	0.833	1.139	1.762	2.220
1.0	0.01	1.661	1.666	1.680	1.689	1.694	1.715	1.747	1.833	1.926
	0.1	1.503	1.510	1.530	1.550	1.571	1.612	1.665	1.781	1.886
	0.2	1.363	1.370	1.394	1.423	1.459	1.516	1.589	1.735	1.854
	0.3	1.252	1.260	1.286	1.322	1.370	1.441	1.531	1.704	1.837
	0.4	1.163	1.173	1.201	1.242	1.299	1.380	1.484	1.683	1.830
	0.5	1.093	1.102	1.132	1.178	1.242	1.332	1.449	1.675	1.838
	0.6	1.036	1.046	1.077	1.127	1.199	1.300	1.432	1.686	1.866
	0.7	0.992	1.003	1.035	1.090	1.172	1.286	1.436	1.722	1.921
	0.8	0.959	0.971	1.005	1.067	1.162	1.295	1.469	1.803	2.031
	0.9	0.940	0.953	0.989	1.063	1.181	1.343	1.572	2.018	2.303
2.0	0.01	1.215	1.209	1.192	1.154	1.099	1.043	0.989	0.964	1.027
	0.1	1.158	1.153	1.139	1.106	1.059	1.012	0.965	0.949	1.014
	0.2	1.100	1.096	1.086	1.059	1.020	0.981	0.943	0.937	1.005
	0.3	1.051	1.048	1.040	1.019	0.987	0.956	0.926	0.929	1.000
	0.4	1.009	1.006	1.001	0.985	0.960	0.935	0.911	0.924	0.998
	0.5	0.973	0.971	0.968	0.956	0.936	0.918	0.900	0.923	1.001
	0.6	0.943	0.941	0.940	0.932	0.918	0.906	0.896	0.929	1.012
	0.7	0.918	0.917	0.917	0.913	0.906	0.901	0.899	0.943	1.032
	0.8	0.899	0.898	0.900	0.902	0.902	0.905	0.913	0.974	1.072
	0.9	0.886	0.886	0.890	0.899	0.912	0.928	0.955	1.056	1.174

Table 12 Dimensionless stress intensity factors for double surface cracks at a hole under wedge loading, r/t=5.0

a/c	a/t	$\varphi°$ 0.1	11.3	22.5	33.8	45.0	56.3	67.5	82.5	89.9
0.2	0.01	0.703	0.828	1.035	1.215	1.362	1.484	1.582	1.688	1.728
	0.1	0.517	0.613	0.776	0.933	1.081	1.228	1.377	1.582	1.678
	0.2	0.403	0.480	0.612	0.747	0.887	1.040	1.213	1.492	1.642
	0.3	0.331	0.397	0.508	0.628	0.761	0.913	1.098	1.428	1.627
	0.4	0.281	0.339	0.435	0.546	0.673	0.824	1.016	1.383	1.628
	0.5	0.244	0.296	0.382	0.486	0.609	0.760	0.958	1.358	1.646
	0.6	0.215	0.263	0.340	0.440	0.562	0.716	0.927	1.361	1.694
	0.7	0.192	0.238	0.308	0.405	0.529	0.692	0.922	1.398	1.780
	0.8	0.175	0.219	0.284	0.380	0.511	0.689	0.950	1.497	1.945
	0.9	0.161	0.207	0.268	0.367	0.512	0.720	1.052	1.775	2.349
0.4	0.01	1.017	1.065	1.185	1.312	1.428	1.531	1.620	1.726	1.773
	0.1	0.865	0.910	1.019	1.144	1.267	1.390	1.508	1.665	1.737
	0.2	0.745	0.785	0.885	1.004	1.131	1.267	1.409	1.613	1.713
	0.3	0.658	0.695	0.786	0.901	1.031	1.175	1.335	1.580	1.706
	0.4	0.592	0.627	0.712	0.824	0.955	1.106	1.279	1.560	1.712
	0.5	0.541	0.575	0.655	0.765	0.898	1.054	1.241	1.558	1.737
	0.6	0.501	0.534	0.611	0.720	0.856	1.022	1.226	1.582	1.790
	0.7	0.469	0.502	0.577	0.688	0.831	1.011	1.238	1.641	1.881
	0.8	0.445	0.479	0.553	0.667	0.823	1.026	1.288	1.764	2.050
	0.9	0.430	0.466	0.539	0.662	0.842	1.083	1.426	2.077	2.454
1.0	0.01	1.689	1.693	1.707	1.712	1.719	1.743	1.774	1.878	2.010
	0.1	1.592	1.597	1.614	1.627	1.644	1.679	1.723	1.843	1.981
	0.2	1.497	1.504	1.523	1.543	1.571	1.617	1.675	1.813	1.958
	0.3	1.417	1.424	1.447	1.474	1.510	1.567	1.637	1.793	1.946
	0.4	1.350	1.358	1.383	1.415	1.460	1.526	1.606	1.780	1.941
	0.5	1.294	1.302	1.329	1.366	1.418	1.492	1.584	1.777	1.948
	0.6	1.248	1.255	1.284	1.327	1.386	1.470	1.576	1.791	1.972
	0.7	1.210	1.218	1.249	1.297	1.365	1.463	1.585	1.824	2.018
	0.8	1.181	1.190	1.224	1.279	1.360	1.474	1.616	1.894	2.110
	0.9	1.163	1.173	1.209	1.276	1.379	1.519	1.710	2.076	2.336
2.0	0.01	1.207	1.201	1.184	1.145	1.090	1.035	0.981	0.956	1.018
	0.1	1.172	1.166	1.151	1.117	1.067	1.016	0.967	0.947	1.011
	0.2	1.136	1.131	1.118	1.087	1.043	0.999	0.955	0.941	1.007
	0.3	1.104	1.100	1.090	1.063	1.024	0.985	0.947	0.940	1.007
	0.4	1.077	1.074	1.065	1.043	1.009	0.975	0.941	0.941	1.011
	0.5	1.054	1.051	1.045	1.026	0.997	0.968	0.940	0.947	1.020
	0.6	1.035	1.032	1.028	1.013	0.990	0.967	0.945	0.961	1.038
	0.7	1.020	1.018	1.016	1.005	0.988	0.973	0.959	0.984	1.067
	0.8	1.010	1.008	1.009	1.004	0.995	0.989	0.985	1.027	1.119
	0.9	1.005	1.005	1.008	1.012	1.017	1.025	1.043	1.127	1.240

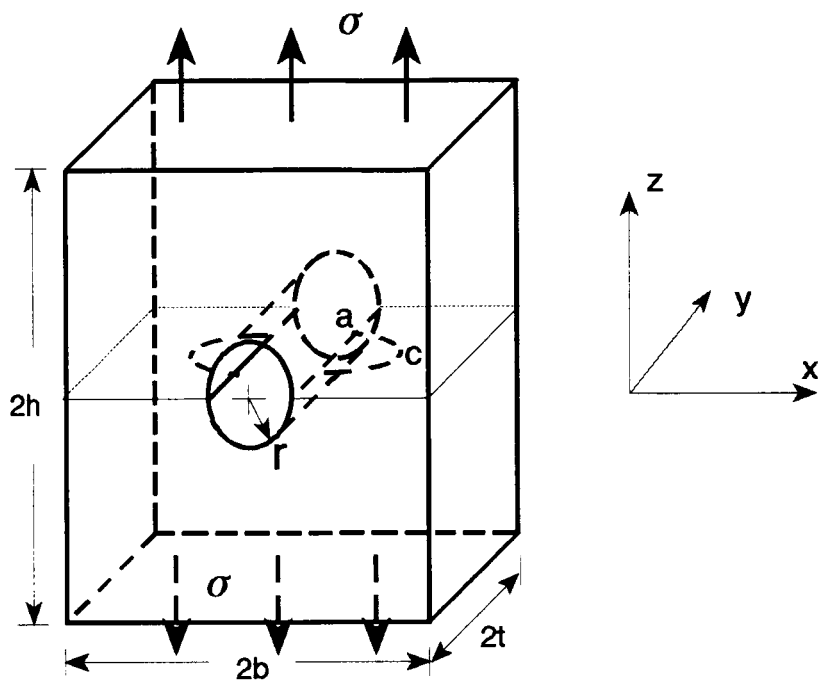

Fig.1 Double surface cracks at a hole under remote tension

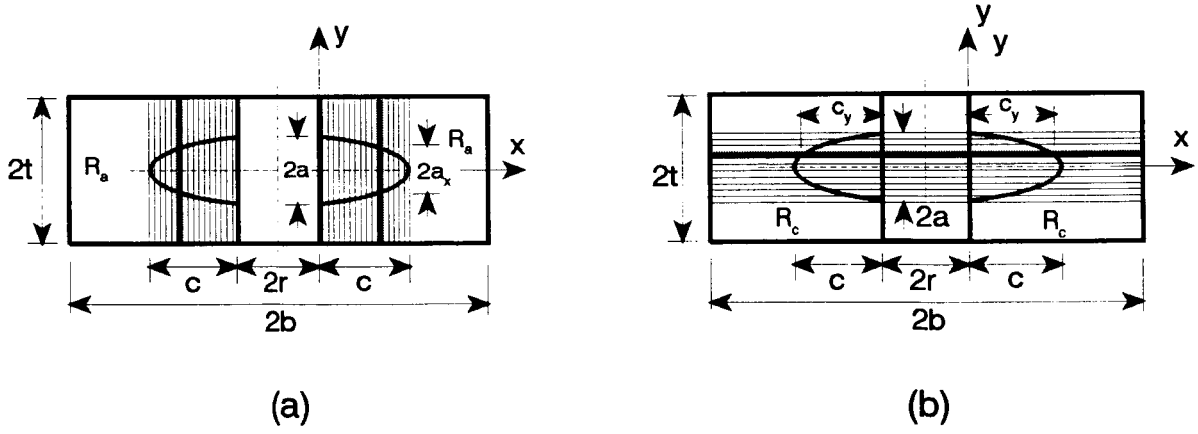

Fig.2 Decomposition of surface cracked body into (a) a-slice, (b) c-slice

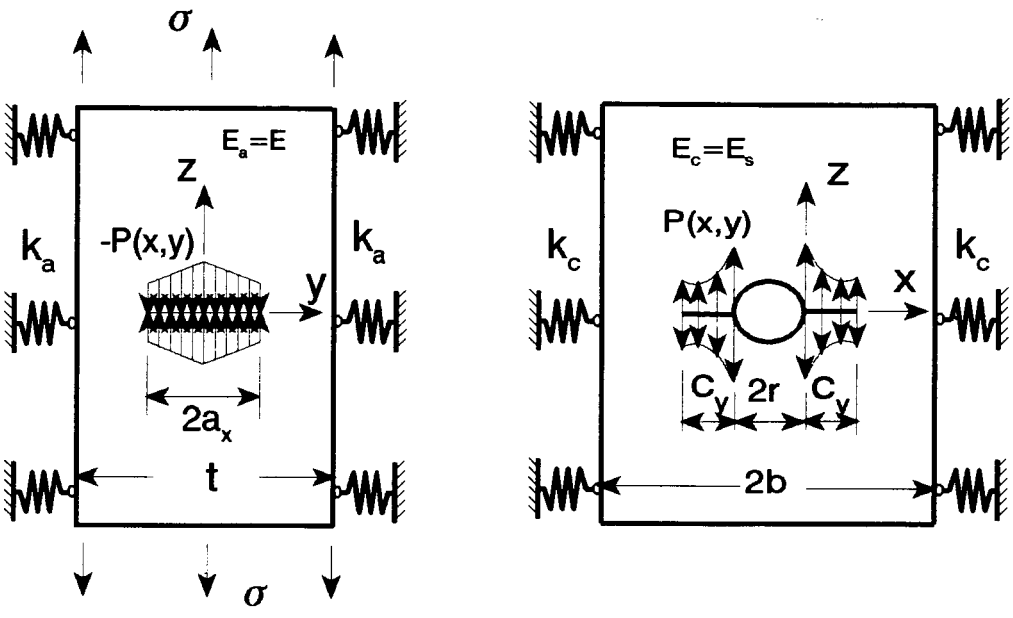

(a) (b)

Fig.3 $0<k_i<\infty$, (a) a-slice, (b) c-slice.

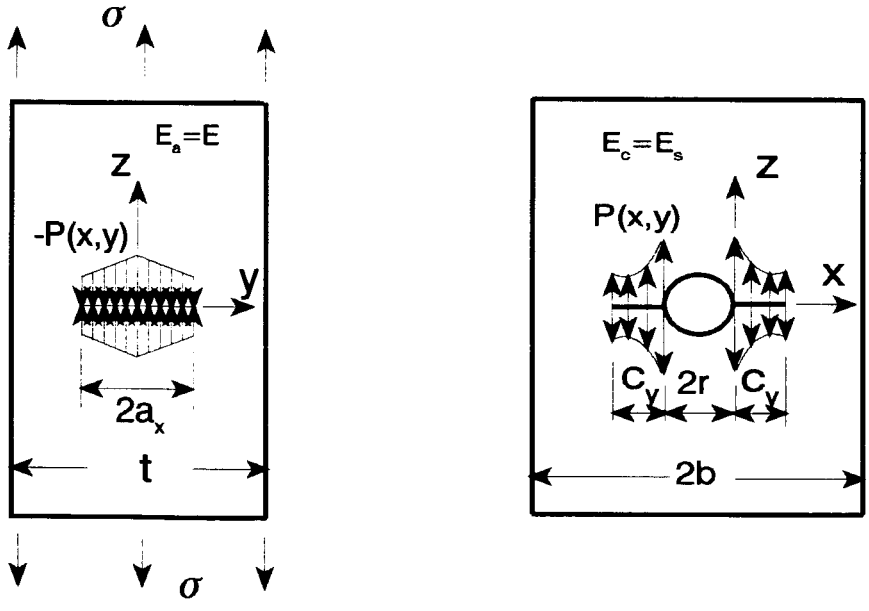

(a) (b)

Fig.4 $k_i=0$, (a) a-slice, (b) c-slice.

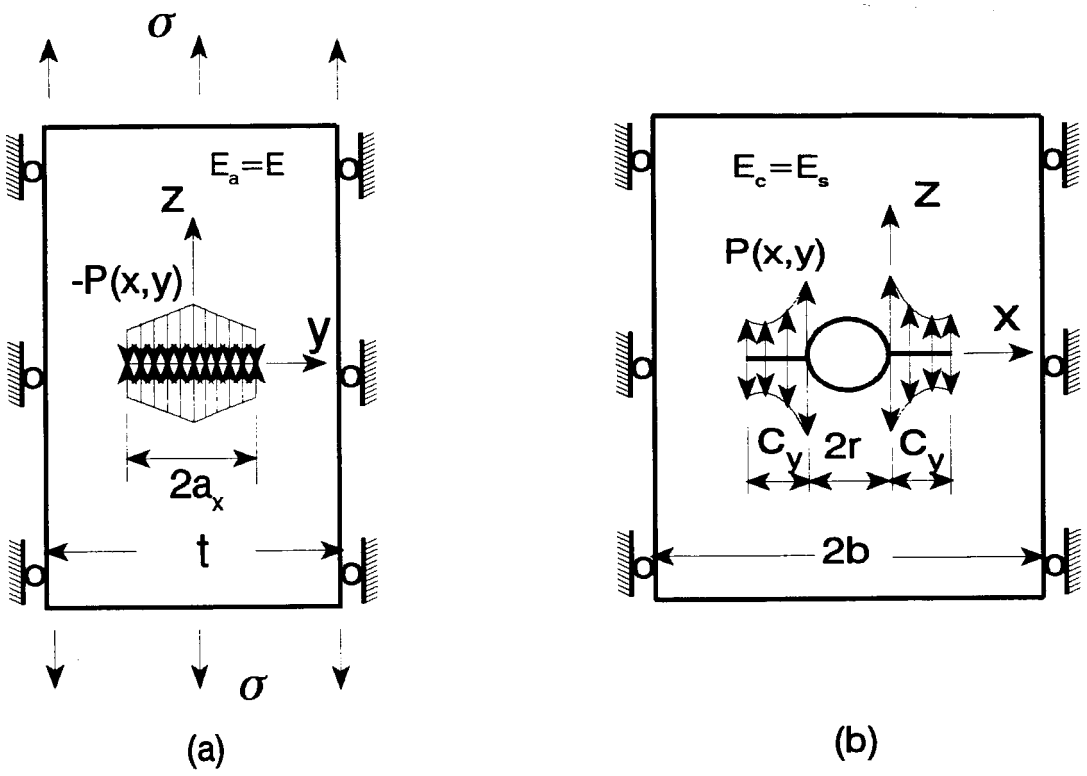

Fig.5 $k_i=\infty$, (a) a-slice, (b) c-slice

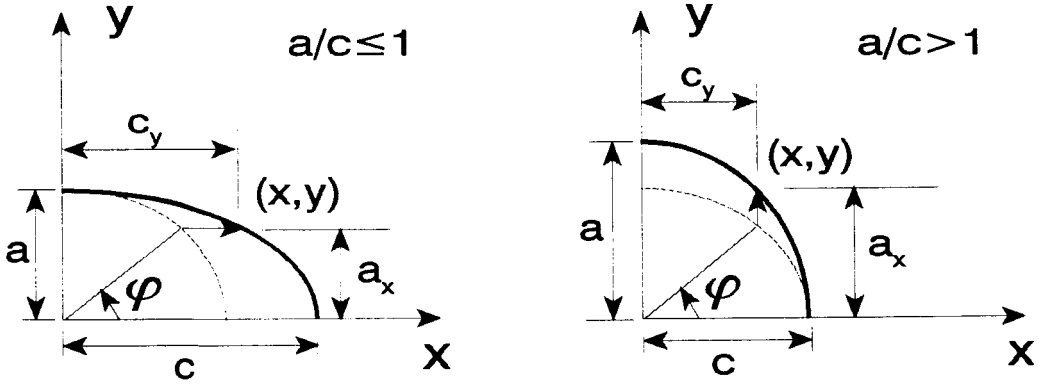

Fig.6 Definition of crack parameters

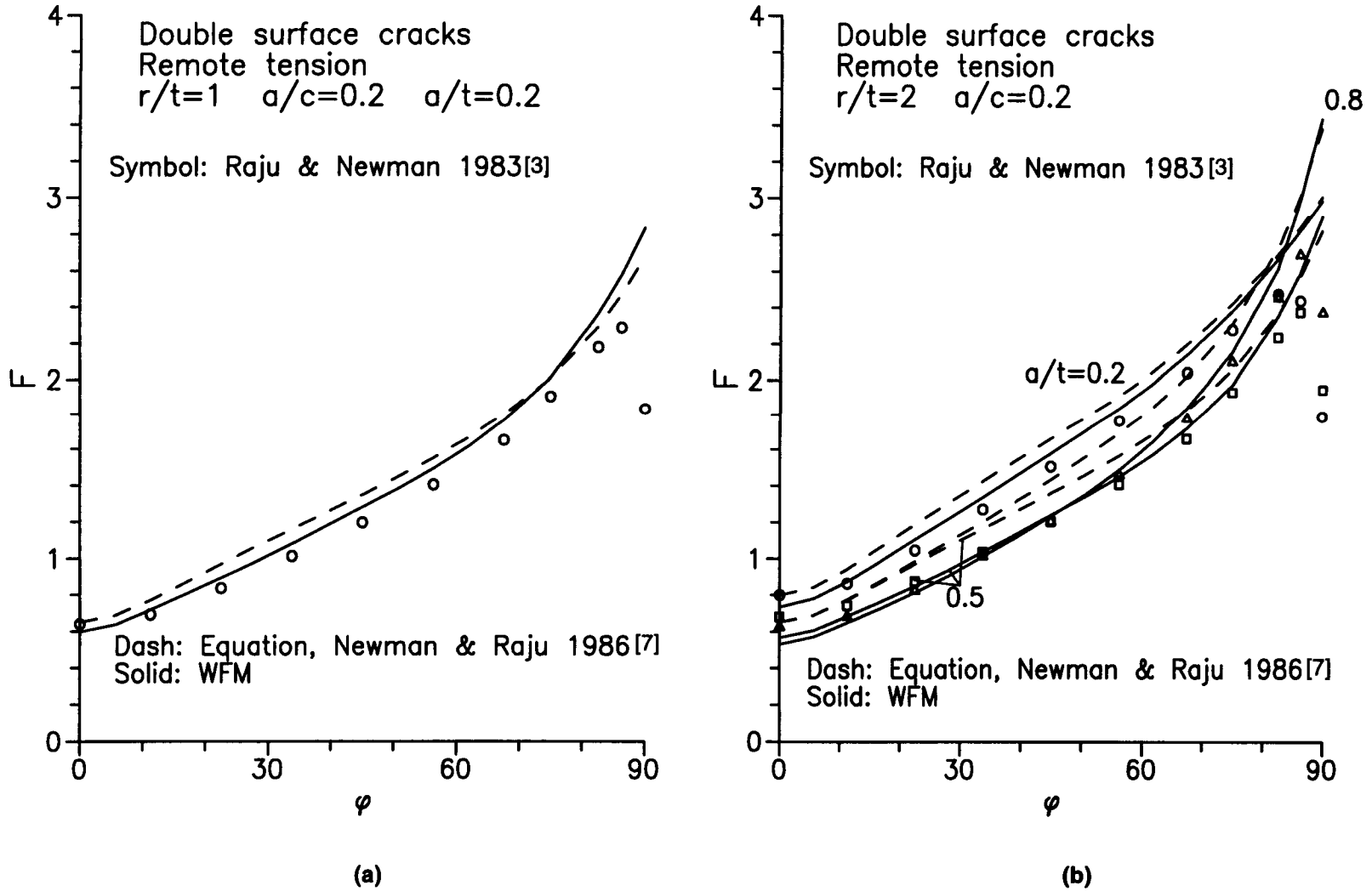

Fig.7 Comparison with finite element solutions for remote tension, a/c=0.2

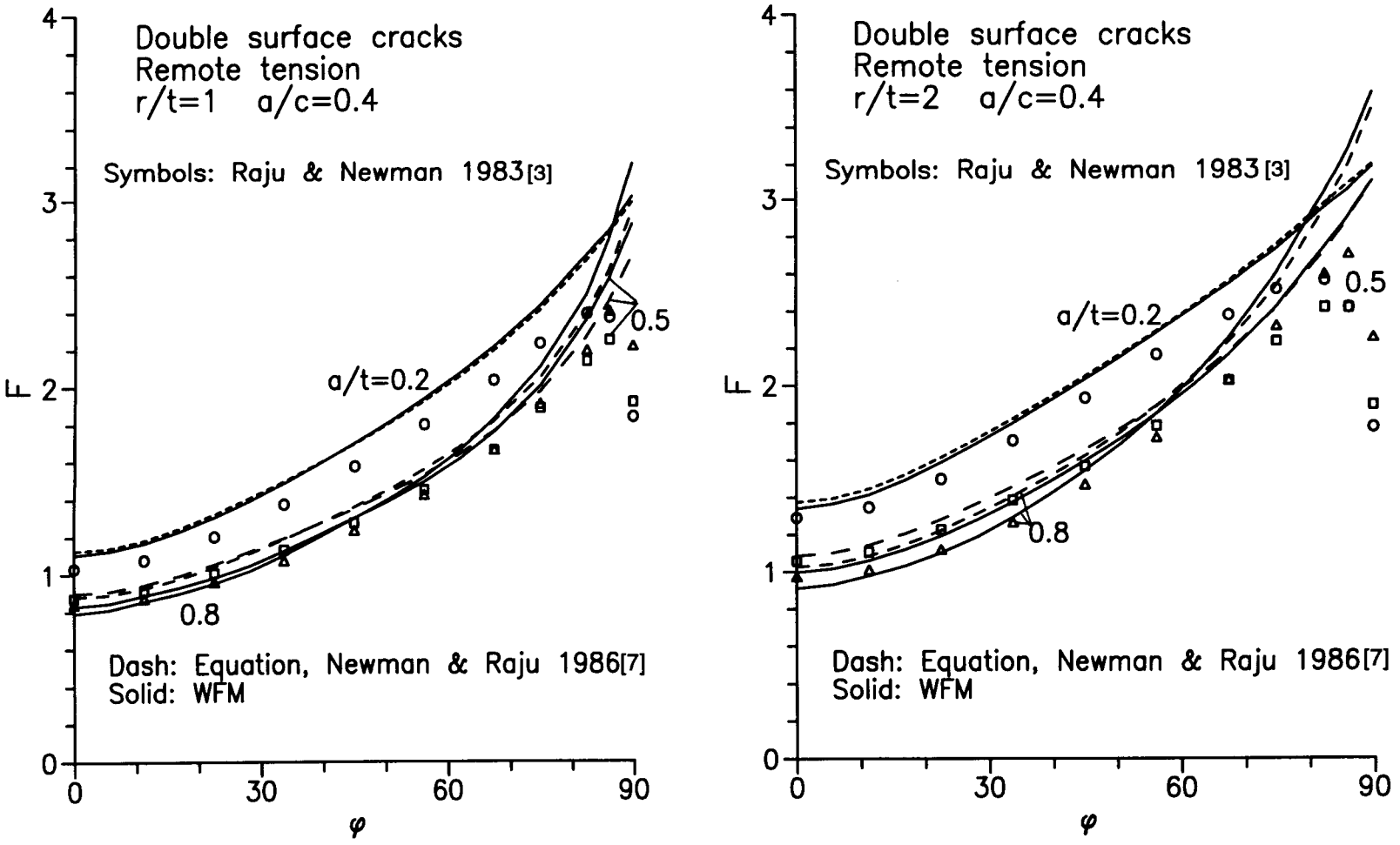

Fig.8 Comparison with finite element solutions for remote tension, a/c=0.4

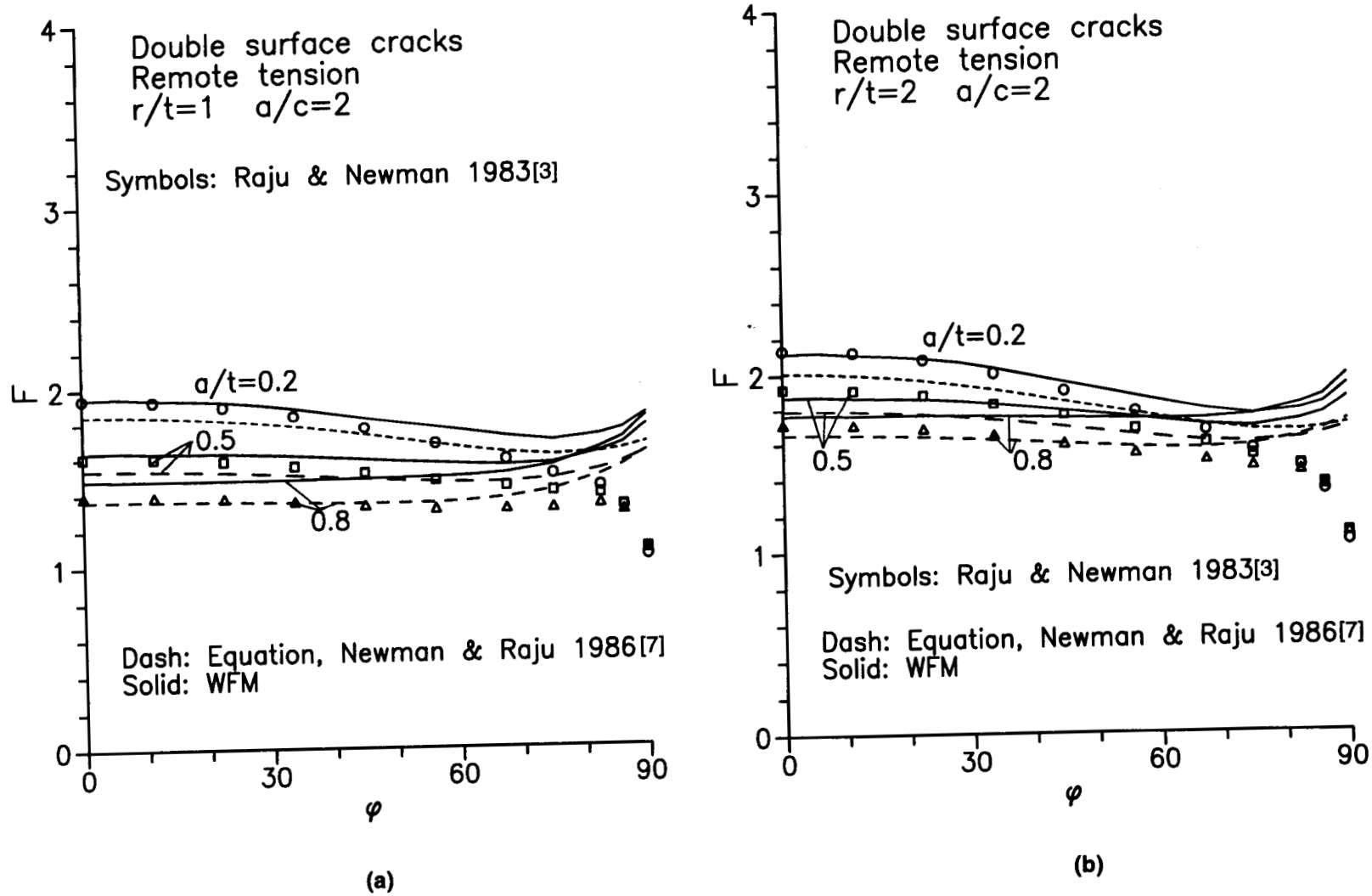

Fig.9 Comparison with finite element solutions for remote tension, a/c=2

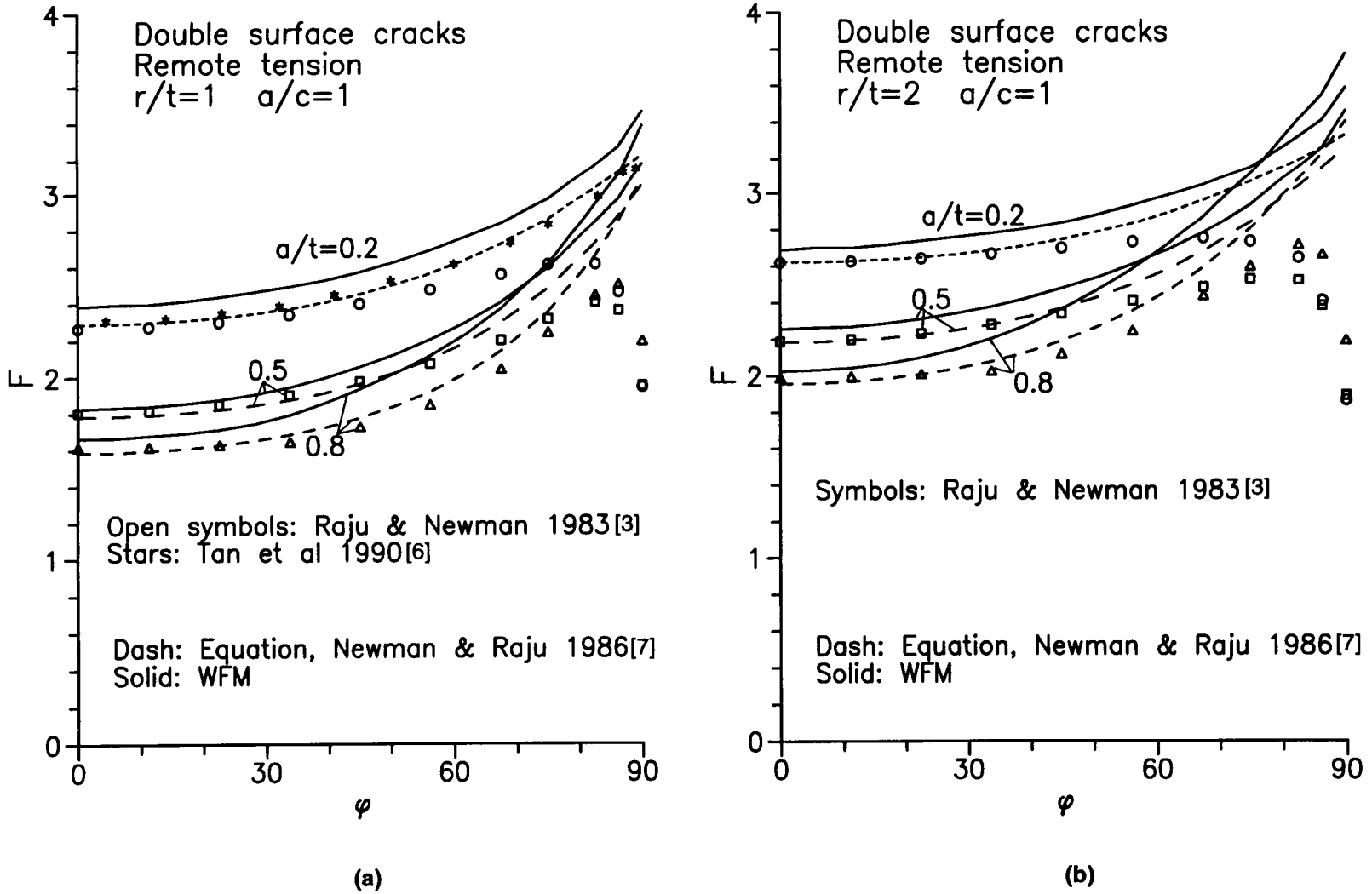

Fig.10 Comparison with finite element solutions for remote tension, a/c=1

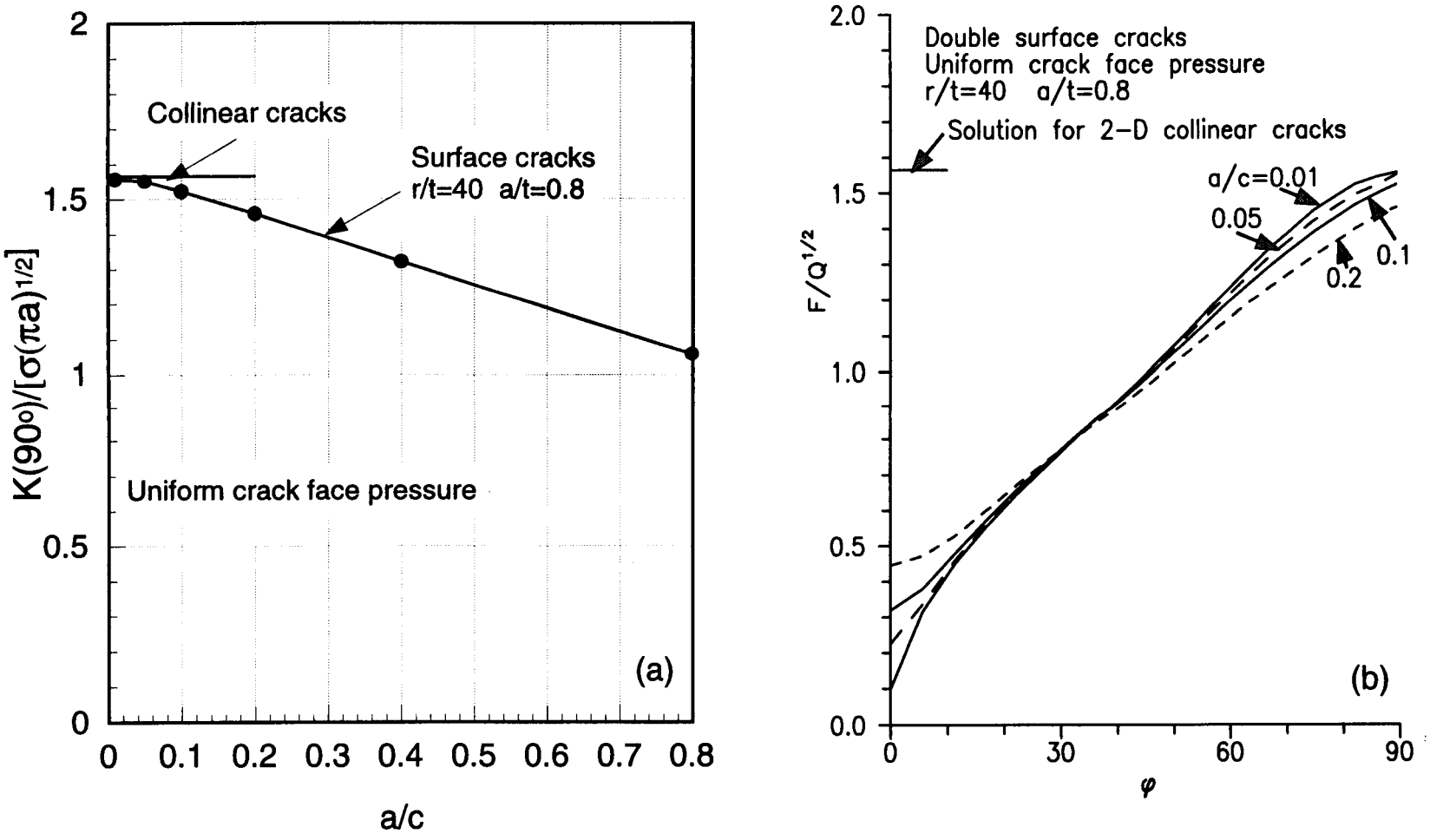

Fig.11 Limiting behavior of stress intensity factors as a/c tends to 0

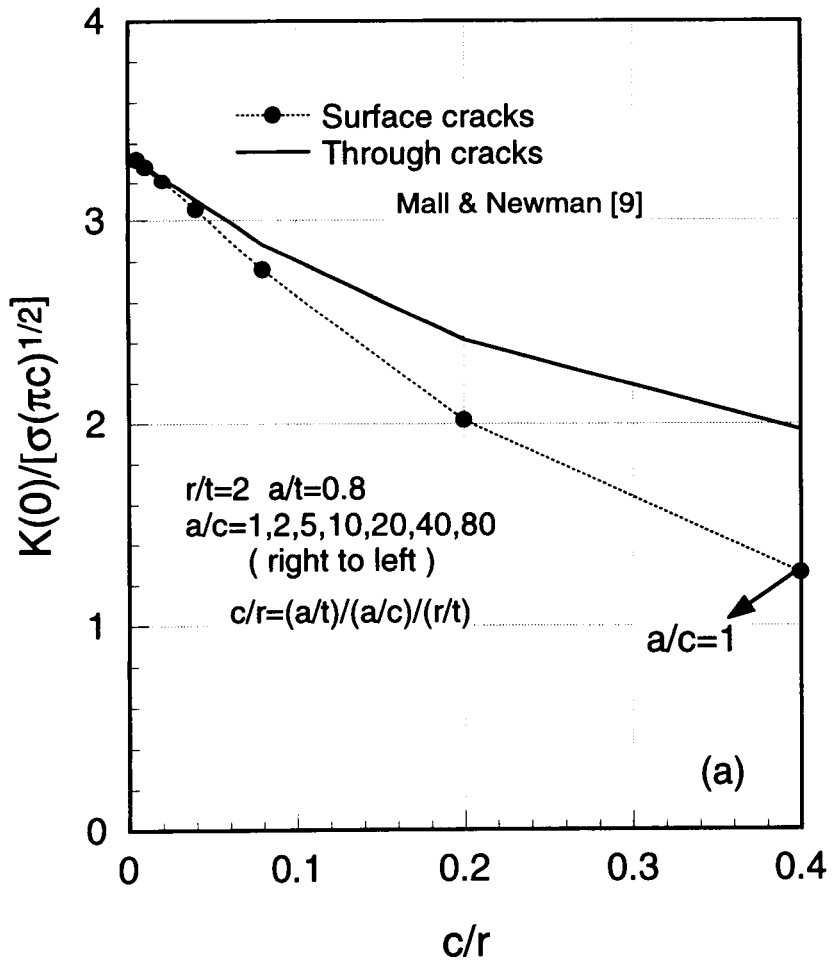

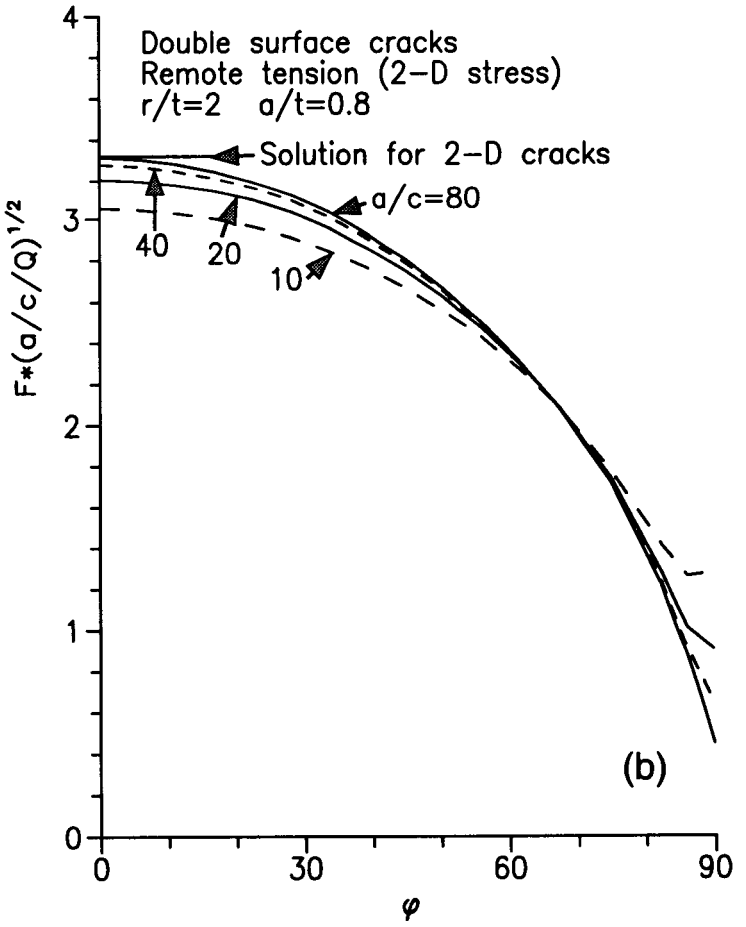

Fig.12 Limiting behavior of stress intensity factors as a/c tends to infinity

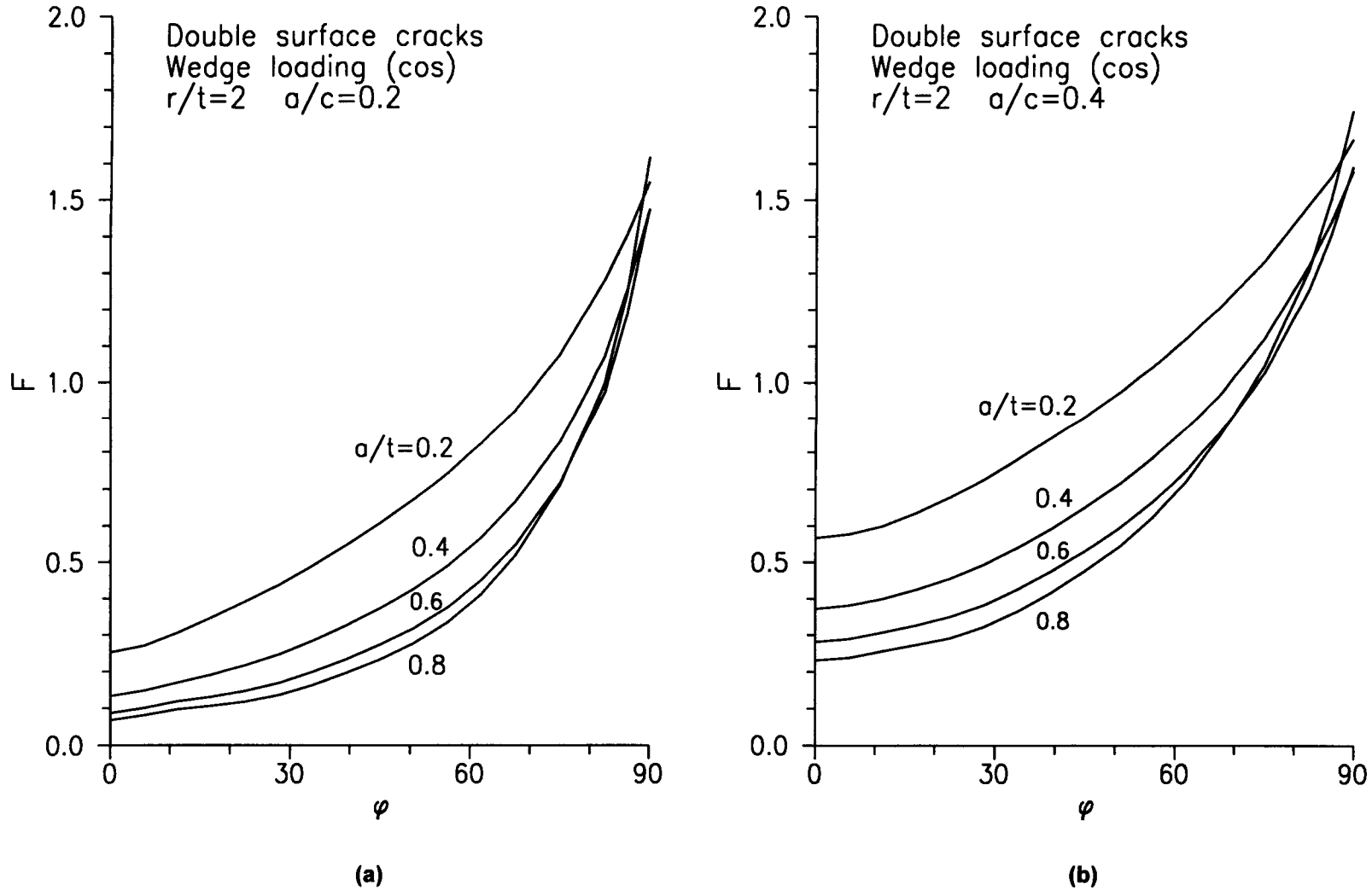

Fig.13 Dimensionless stress intensity factors for wedge loading in the hole

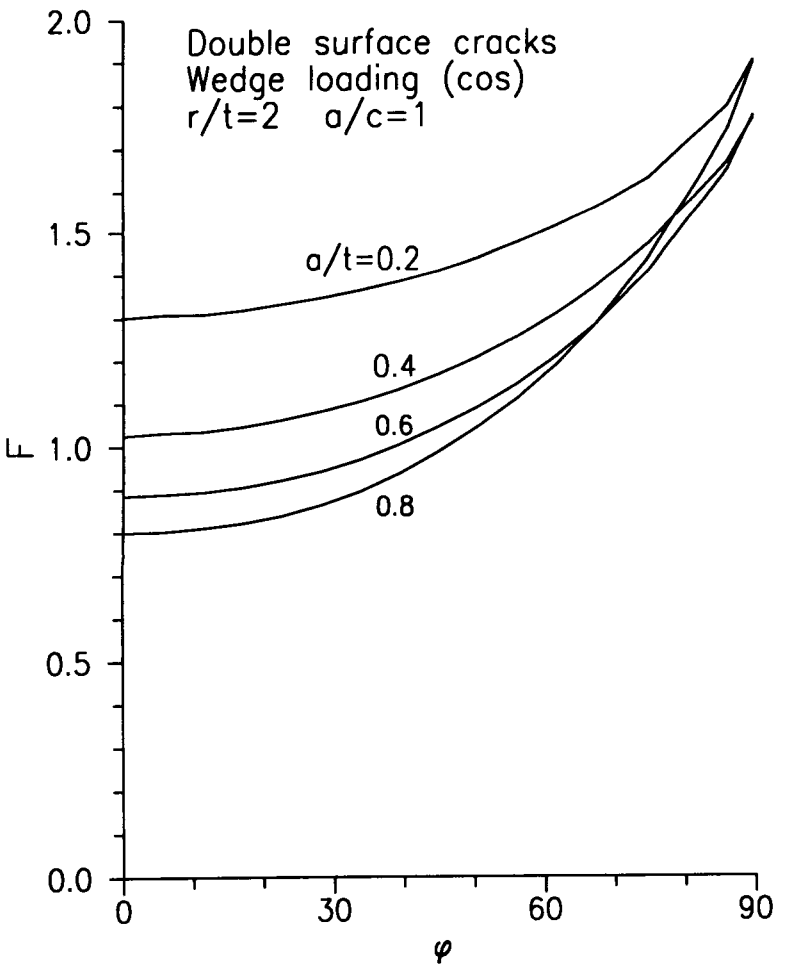

(c)

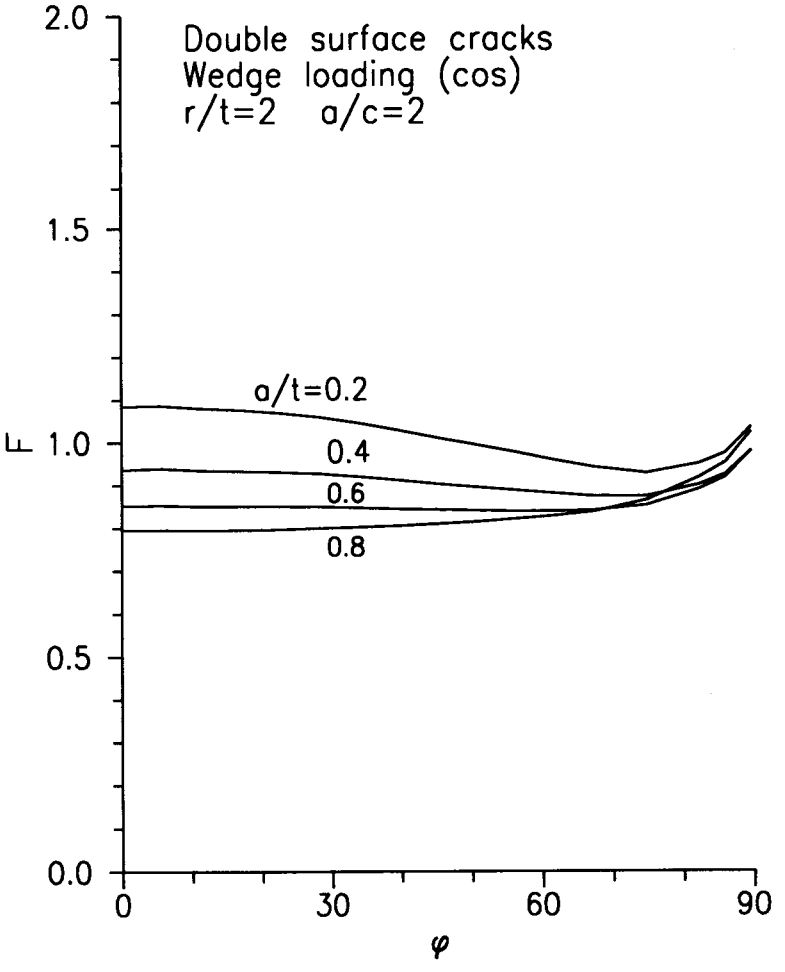

(d)

Fig.13 (continued)

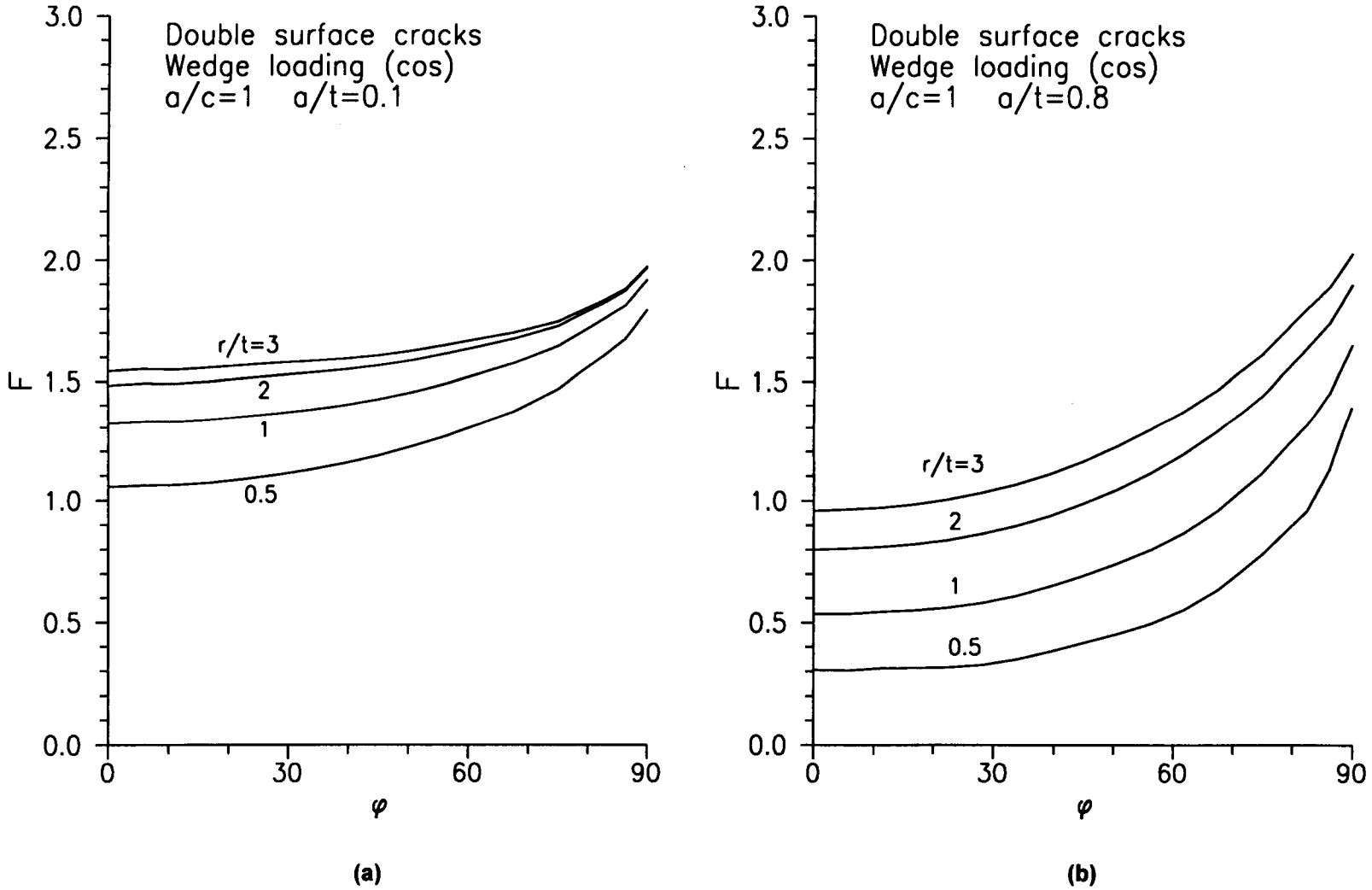

Fig.14 Influence of hole radius on the stress intensity factors for wedge loading

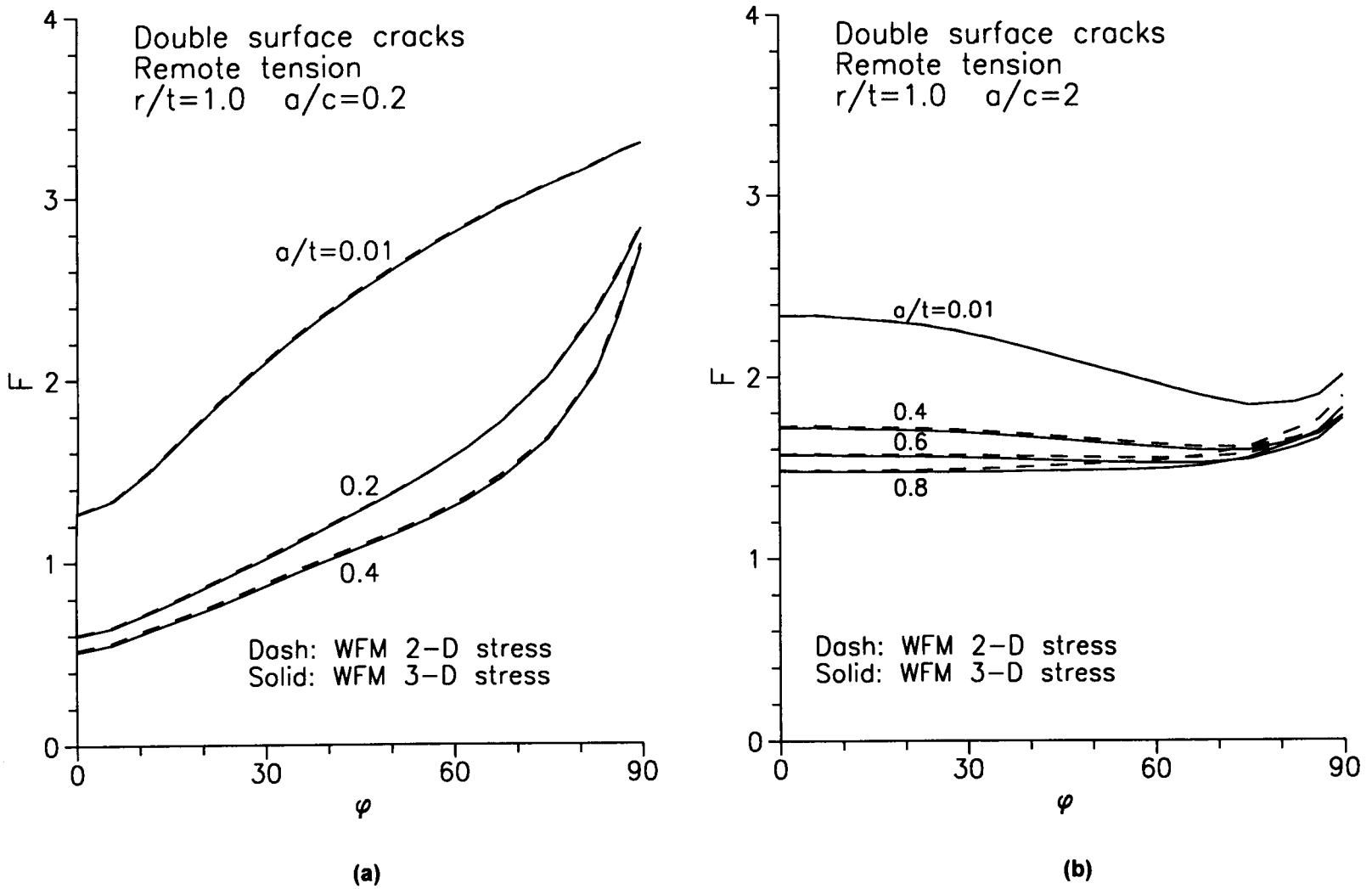

Fig. 15 Comparison of solutions obtained by using 2-D and 3-D stress distributions

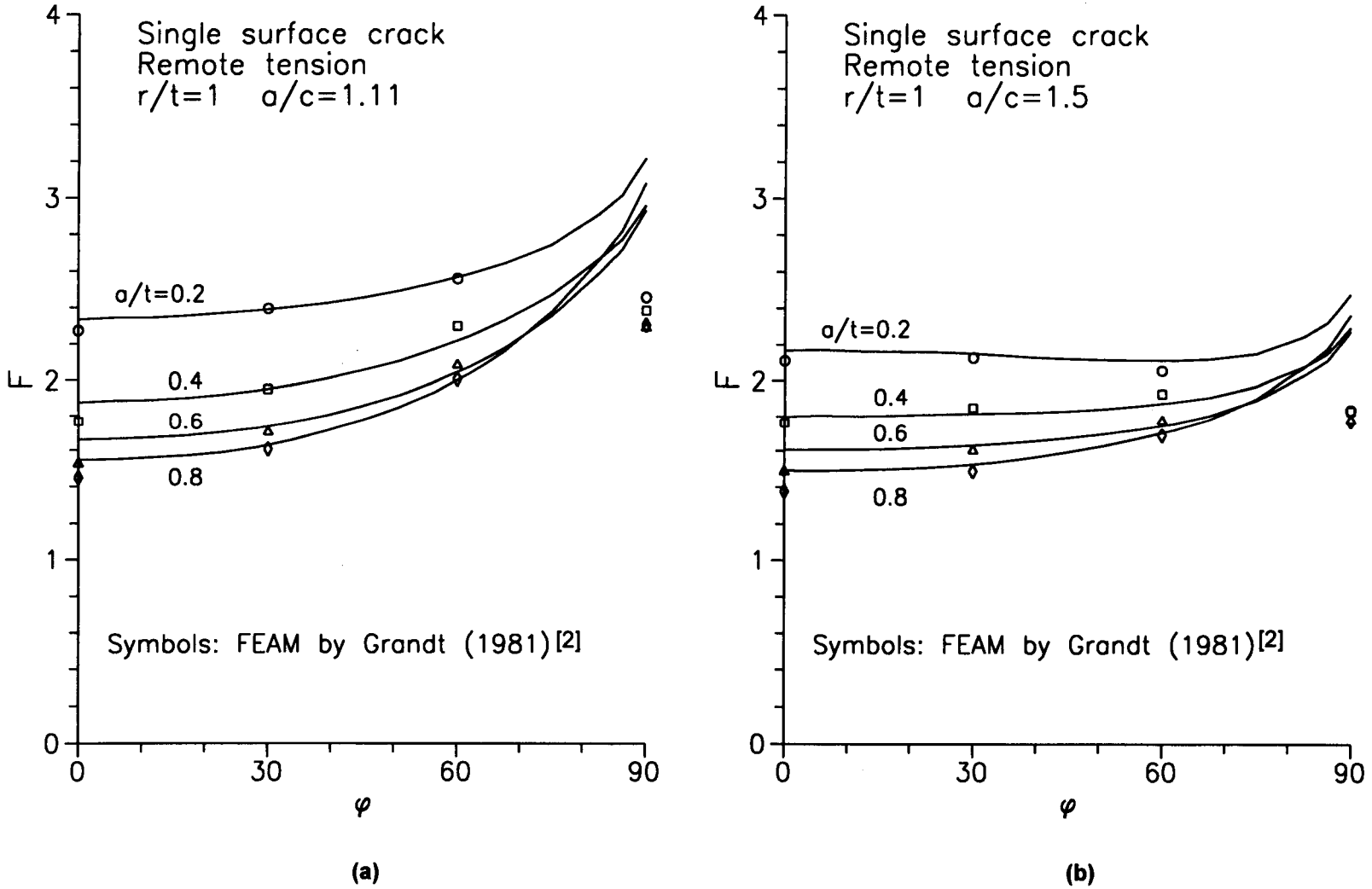

Fig.16 Comparison with finite element alternating solutions for single crack under remote tension

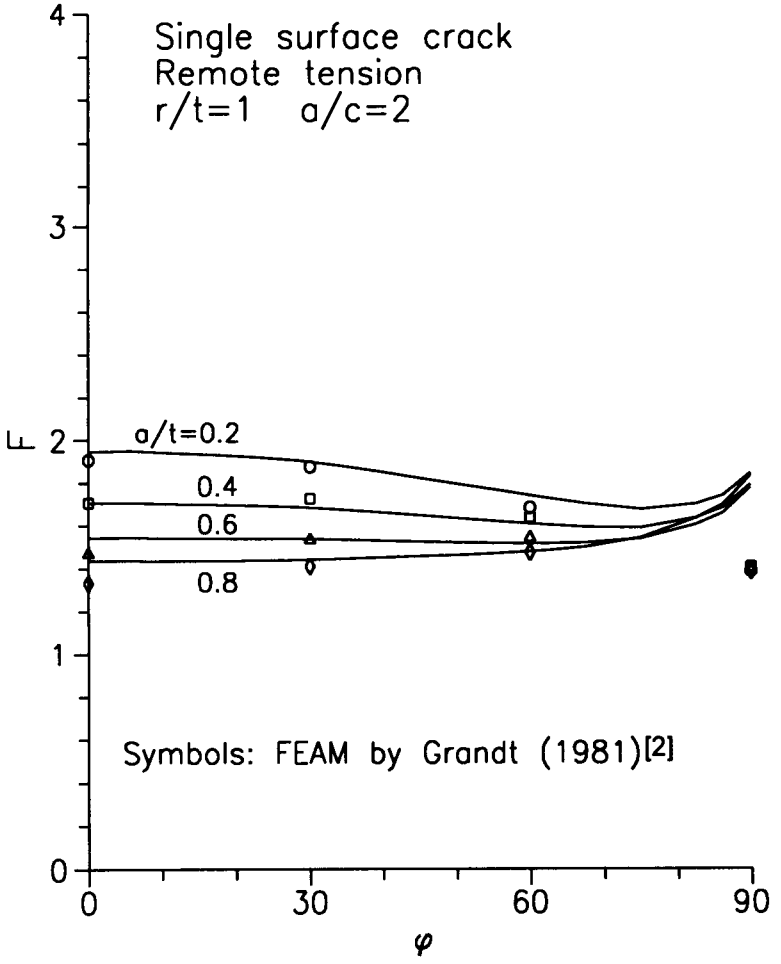

(c)

Fig.16 (continued)

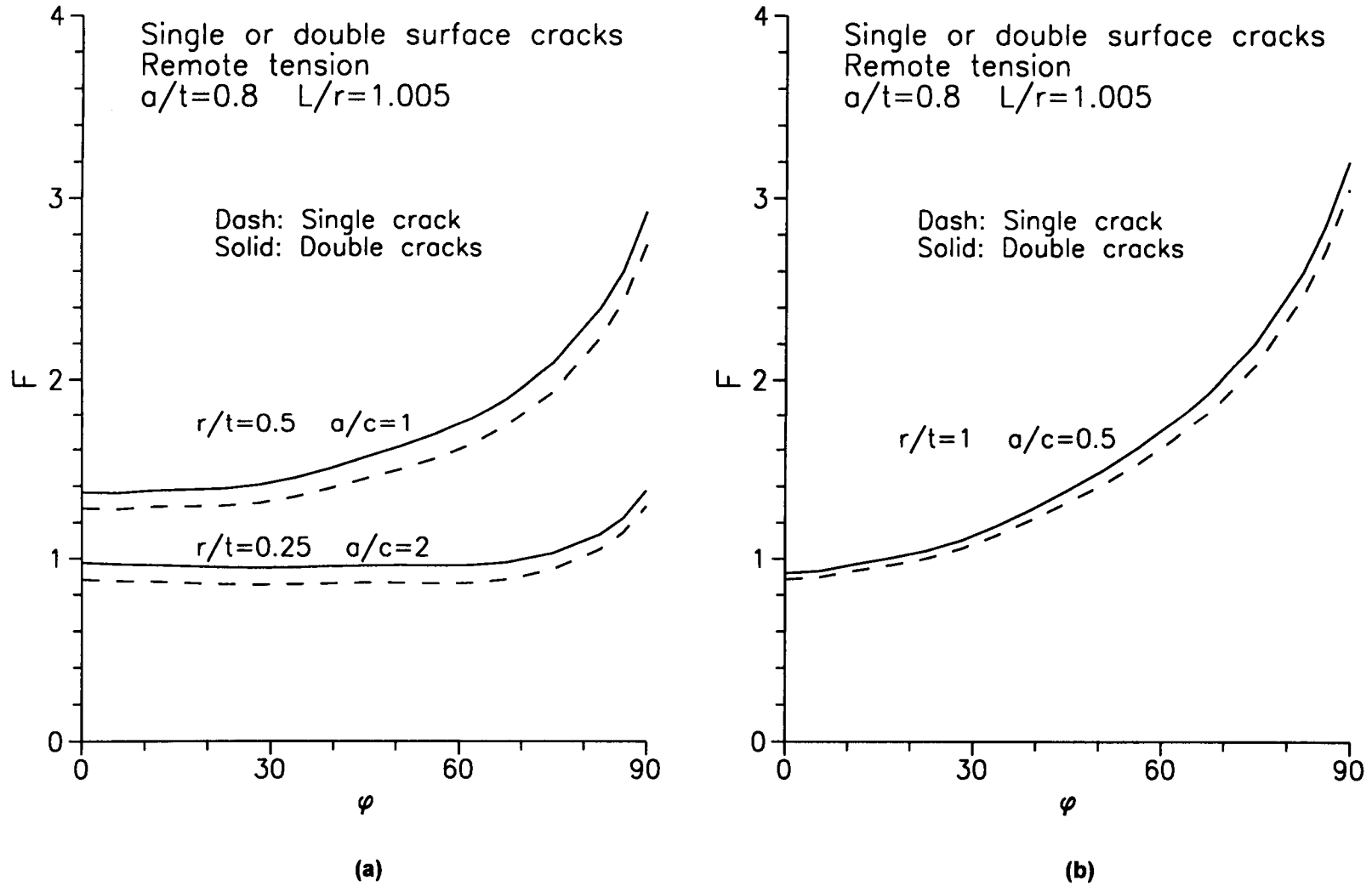

Fig.17 Comparison between single crack and double cracks for remote tension

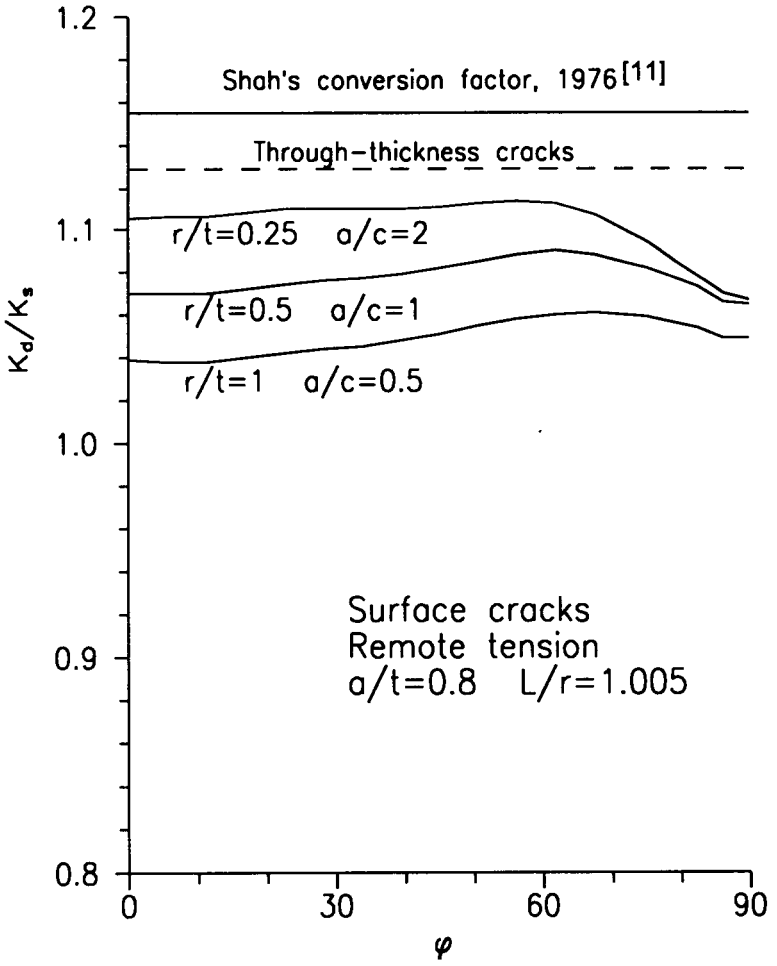

(c)

Fig.17 (continued)

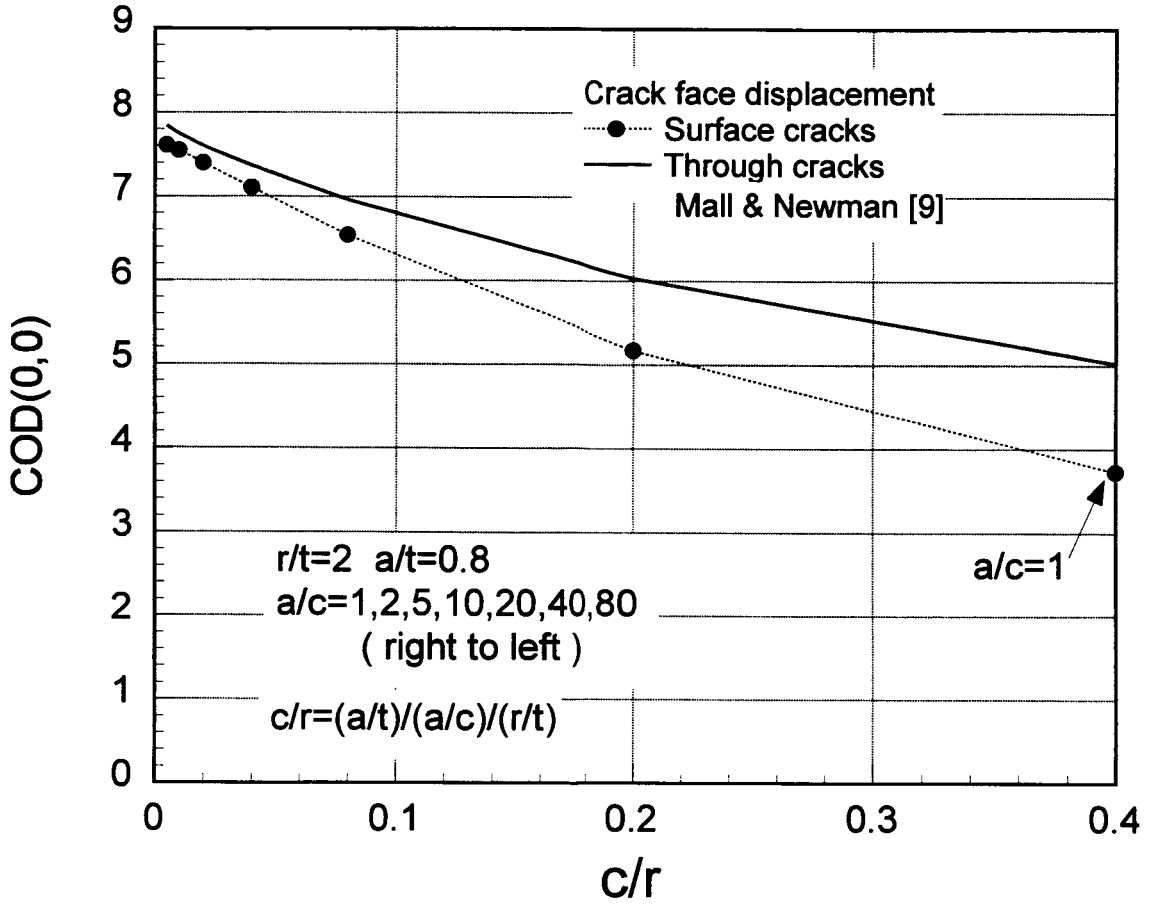

Fig.18 Normalized crack mouth displacements for remote tension

REPORT DOCUMENTATION PAGE

Form Approved
OMB No. 0704-0188

1. AGENCY USE ONLY (*Leave blank*)	2. REPORT DATE	3. REPORT TYPE AND DATES COVERED
	July 1995	Technical Memorandum

4. TITLE AND SUBTITLE
Analysis of Surface Cracks at Hole by a 3-D Weight Function Method with Stresses from Finite Element Method

5. FUNDING NUMBERS
WU 538-02-10-01

6. AUTHOR(S)
W. Zhao, J. C. Newman, Jr., M. A. Sutton, K. N. Shivakumar, and X. R. Wu

7. PERFORMING ORGANIZATION NAME(S) AND ADDRESS(ES)
NASA Langley Research Center
Hampton, VA 23681-0001

8. PERFORMING ORGANIZATION REPORT NUMBER

9. SPONSORING / MONITORING AGENCY NAME(S) AND ADDRESS(ES)
National Aeronautics and Administration
Washington, DC 20546-0001

10. SPONSORING / MONITORING AGENCY REPORT NUMBER
NASA TM-110145

11. SUPPLEMENTARY NOTES
Zhao: University of South Carolina, Columbia, SC; Newman: Langley Research Center, Hampton, VA; Sutton: University of South Carolina, Columbia, SC; Shivakumar: North Carolina A&T State University, Greensboro, NC; Wu: Institute of Aeronautical Materials, Beijing, Peoples Republic of China

12a. DISTRIBUTION / AVAILABILITY STATEMENT
Unclassified - Unlimited

Subject Category 24

12b. DISTRIBUTION CODE

13. ABSTRACT (*Maximum 200 words*)

Parallel with the work in Part-I, stress intensity factors for semi-elliptical surface cracks emanating from a circular hole are determined. The 3-D weight function method with the 3-D finite element solutions for the uncracked stress distribution as in Part-I is used for the analysis. Two different loading conditions, i.e. remote tension and wedge loading, are considered for a wide range in geometrical parameters. Both single and double surface cracks are studied and compared with other solutions available in the literature. Typical crack opening displacements are also provided.

14. SUBJECT TERMS
Stress-intensity factors; Weight functions; Finite-element method; Corner crack

15. NUMBER OF PAGES
42

16. PRICE CODE
A03

17. SECURITY CLASSIFICATION OF REPORT	18. SECURITY CLASSIFICATION OF THIS PAGE	19. SECURITY CLASSIFICATION OF ABSTRACT	20. LIMITATION OF ABSTRACT
Unclassified	Unclassified		